Available online at www.sciencedirect.com
ScienceDirect
ELSEVIER
Nuclear Physics A 777 (2006) 254–290
NUCLEAR PHYSICS A

Nuclear reactions in stellar helium burning and later hydrostatic burning stages

L.R. Buchmann [a,*], C.A. Barnes [b]

[a] *TRIUMF, Vancouver, BC, V6T 2A3, Canada*
[b] *California Institute of Technology, Pasadena, CA 91125, USA*

Received 17 September 2004; received in revised form 13 December 2004; accepted 4 January 2005

Available online 21 January 2005

Abstract

We review in some detail, the so-called triple-α process and the reaction $^{12}C(\alpha,\gamma)^{16}O$ that follow core hydrogen burning and produce most of the universal abundances of ^{12}C and ^{16}O, including considerable new and previously unpublished work. We also review briefly, for reasons of length, some of the principal nuclear reactions involved in carbon burning, neon burning, oxygen burning, the reactions generally grouped under the title silicon burning, and the helium-induced reactions that produce neutrons to build the s-process nuclei.

1. Introduction

After hydrogen burning in the core of a star, the core is transformed mainly to ^{4}He, and H-burning continues in a shell surrounding the core, adding more helium to the core. Without the core energy production, the centre of the star will undergo some contraction, and the temperature of the core will rise. Meanwhile the outer layers of the star expand to become a red giant. However, the internal support of the star against gravity may continue

* Corresponding author.
E-mail address: lothar@triumf.ca (L.R. Buchmann).

0375-9474/$ – see front matter
doi:10.1016/j.nuclphysa.2005.01.005

to be augmented by electron degeneracy[1] in the ^{4}He core as the pressure rises, while the main energy source remains the H-burning shell. At some point the temperature of the core becomes high enough to ignite He-burning, typically with one or more flashes as the electron degeneracy pressure is overcome, and the stellar structure support is supplied by thermal pressure generated by both the He-burning core and the surrounding H-burning shell.

For most of the successive hydrostatic burning stages, the burning processes are ordered to a large extent by the increasing Coulomb barrier that must be overcome by the energy producing nuclear reactions. However, during He-burning, the triple-α (Section 2) and the ^{12}C$(\alpha,\gamma)^{16}$O reactions (Section 3) can proceed simultaneously, with the resulting carbon-oxygen ratio at the end of core He-burning depending on the relative rates of the two reactions as a function of temperature and density, which in turn depend on the initial stellar mass. The carbon-oxygen ratio at the end of helium burning is important in determining the course of later nucleosynthesis in a massive star[2] and the type of remnant left after a supernova stage or, for a less massive star, for the composition of the remnant white dwarf.

Core helium burning is essentially limited to the triple-α and ^{12}C$(\alpha,\gamma)^{16}$O reactions, because the reaction ^{16}O$(\alpha,\gamma)^{20}$Ne has a very low cross section at helium burning temperatures. The low cross section of the ^{16}O$(\alpha,\gamma)^{20}$Ne reaction has been recently confirmed experimentally at the Institut für Strahlenphysik at the University of Stuttgart [2]. The reason for the low cross section is the absence of any state of ^{20}Ne with appropriate spin and parity, near the $^{16}\mathrm{O}+\alpha$ threshold, that could serve as a resonance. Instead, the cross section at low α energies would have to depend on the low energy tails of distant higher energy states in ^{20}Ne, and non-resonant radiative capture, both of which are calculated to give very small yields at He-burning temperatures.

The next burning process after the core He-burning has consumed the helium, and the temperature rises sufficiently is carbon burning (Section 5.1), which converts most of the carbon present in the core to a range of nuclei from neon to phosphorous, with ^{20}Ne and ^{24}Mg being the dominant nuclear products, along with unburned ^{16}O.

It might seem reasonable that oxygen burning would be the next process, but there is an intermediate stage, neon burning (Section 5.2), that occurs earlier because the rising temperature and the unusually low α-particle binding energy in ^{20}Ne cause the ^{20}Ne to be photodisintegrated to ^{16}O and an α-particle. The α particle released can then combine with ^{20}Ne to form ^{24}Mg with a slight net energy gain. The overall nucleosynthesis results are similar to carbon burning.

Oxygen burning (Section 5.3), the next process, together with protons, neutrons and α-particles liberated by photodisintegration of nuclei produced by previous processes will build a range of nuclei from ^{28}Si to ^{50}Cr, with ^{28}Si and ^{32}S as the principal results.

Silicon burning (Section 5.4) is the name given to the complex of reactions of α-particles, protons, and neutrons with the nuclei present after oxygen burning. The source of the α-particles, protons and neutrons continues to be the photodisintegration of the most abundant nuclei present, and the build-up of heavier nuclei continues until most of the

[1] The degree of degeneracy depends on the stellar mass and is high for low mass stars while massive stars do not reach degeneracy [1].

[2] The stellar mass beyond which stellar evolution continues beyond helium burning is around 8 solar masses.

nuclei in the core are iron or nickel isotopes, in the region of nuclei with the maximum binding energy per nucleon.

Because of the increasing Coulomb barrier above the iron abundance peak, and also because the energy required to photodisintigrate the iron peak nuclei, to obtain neutrons and protons to build still heavier nuclei is more than the energy gained per nucleon captured, the iron peak is essentially the end of the hydrostatic burning stages, and some of the heavier elements must be the result of slow successive radiative capture of neutrons on iron or capture by heavier nuclei beyond the iron abundance peak that were present initially in the star.[3] The nuclear reactions that produce these neutrons for the s-process are most likely the He-shell burning reactions $^{13}\mathrm{C} + {}^{4}\mathrm{He} \rightarrow \mathrm{n} + {}^{16}\mathrm{O}$ and $^{22}\mathrm{Ne} + {}^{4}\mathrm{He} \rightarrow \mathrm{n} + {}^{25}\mathrm{Mg}$. The mechanisms of these reactions are discussed elsewhere in this article (Section 4).

2. The triple-alpha process

2.1. The $E_x = 7.654$ MeV state of ^{12}C

As noted above, after core hydrogen burning, the core of a star is mainly helium, with small amounts of other elements present left over from the hydrogen burning or from the materials from which the star formed. To produce more energy in the core, to stabilize the star against contraction, the $A = 5$ and $A = 8$ stable mass gaps have to be bypassed somehow. How this is accomplished by the triple-α process, in which a tiny equilibrium abundance of the unstable nucleus ^{8}Be combines radiatively with a third α particle to form an excited nucleus of ^{12}C, is now a well-known story [3]. In addition, the prediction and experimental verification that there must be a $J^{\pi} = 0^{+}$ excited state of ^{12}C close to the $\alpha + {}^{8}$Be threshold to serve as a resonance, ranks as one of the earlier triumphs of nuclear astrophysics [3].

This state is located at an excitation energy, $E_x = 7.654$ MeV in ^{12}C, and the rate of conversion of ^{4}He to ^{12}C depends entirely on the properties of this resonance state. The quantities needed to determine the rate are the ratios $\Gamma_{\mathrm{rad}}/\Gamma$ and $\Gamma_{e^+e^-}/\Gamma$ and, of course, the energies $[{}^{8}\mathrm{Be} - 2\alpha]$ and $[E_{\mathrm{res}} - ({}^{8}\mathrm{Be} + \alpha)]$. Here Γ is the total of $\Gamma_{\alpha} + \Gamma_{\mathrm{rad}} = \Gamma_{\alpha} + \Gamma_{e^+e^-} + \Gamma_{\gamma}$, where $\Gamma_{e^+e^-} \ll \Gamma_{\gamma} \ll \Gamma_{\alpha}$. It follows that $\Gamma_{\alpha} \approx \Gamma$.

The pair production decay width $\Gamma_{e^+e^-}$ to the ^{12}C ground state can be related directly to inelastic electron scattering from ^{12}C with low momentum transfer q^2. The transition matrix element for this decay is derived [4] by obtaining the elastic and inelastic (longitudinal, Coulomb) form factors, constructing a particular ratio of the two as a function of the momentum transfer q^2 and finding the intercept for zero momentum transfer from higher q^2 data. This form factor function and q^2 have a linear relationship in first order. The validity of this method requires that the transverse (real photon exchange) form factors are small, that the Born approximation is valid for small q^2, and that two step processes in electron scattering can be ignored.

[3] About half of the heavy elements are produced by rapid neutron capture far off the line of nuclear stability.

The error determined for the pair production width is of the order of 6.4%, averaged over three measurements. For the ratio $\Gamma_{e^+e^-}/\Gamma$ the error is 10.3% involving three measurements and, for the ratio $\Gamma_{\rm rad}/\Gamma$, it is 2.7% for seven measurements. The combined error in the radiative width is then 12.5%. Clearly a better determination of the ratio $\Gamma_{e^+e^-}/\Gamma$ would yield great improvement in the stellar reaction rate for static helium burning. However, it would be desirable to obtain a measurement of one of the absolute numbers independent of the electron scattering experiments. To improve the knowledge of this resonance to a level of 5% precision as desired by stellar modelers [5], all three measurements need improvement. Data reevaluations and planned experiments will lead to better determinations of this [6] and other widths [7] in the triple α reaction.

It is interesting to note in passing that the central value of the total width, i.e., the α-width, of $\Gamma_\alpha = 8.9 \pm 1.1$ eV cannot be reasonably produced with an R-matrix formalism for the usual "best" nuclear radius, $a = 1.4(4^{1/3} + 8^{1/3}) = 5.02$ fm, but requires a larger interaction radius of about $a = 6$ fm.

2.2. The triple-α cross section at very high and low temperatures

For temperatures, where the 7.654 MeV state is outside the *Gamow window* relative little information exists about the radiative capture of α-particles on ^{8}Be. This is largely due to the fact that all states of $T = 0$ known above the 7.654 MeV state decay with high probability into 3 α-particles, but with minuscule strength via γ-decay. In addition, the capture cross section is continuous as a function of energy and, in principle, composed of many coherent and incoherent fractions whose strengths and interference patterns are likely unpredictable.

2.2.1. The s-wave

Besides the 7.654 MeV state in ^{12}C there are likely other states contributing to the $J^\pi = 0^+$ strength. A prime candidate is the state at $E_x = 10.3$ MeV in ^{12}C which was assigned a spin and parity of 0^+ or 2^+ in Ref. [8]. However, from angular distributions in transfer reactions and a recent β-delayed α decay study of ^{12}N and ^{12}B [9] a spin assignment of 0^+ is likely. The state has been observed to have a particle width of about $\Gamma_\alpha = 3$ MeV which would provide a long tail reaching into the low energy region. Of course, the γ-strength of this state is completely unknown. Very few natural parity states with isospin zero are indeed seen at higher excitations in ^{12}C. Any such state will have a very large width which may make it unobservable; any 0^+ strength that exists above the 10.3 MeV state will likely form a rather smooth continuum. In addition, regarding the low energy cross section, direct E2 capture is possible to the $E_x = 4.44$ MeV state ($J^\pi = 2^+$)[4] of ^{12}C from the incident s-wave.

[4] As a matter of convenience we will frequently eliminate the leading J^π when spins and parities of states in nuclei are quoted.

2.2.2. Other partial waves

For higher temperatures, certainly other partial waves than the s-wave can become important. However, information is limited about the extent of continuous strength in regions outside resonances. Typically, these resonances are above any reasonable Gamow peak temperature. For the p-wave there is a level at $E_x = 10.844$ MeV with a reported width of $\Gamma = 315$ keV [8]. Certainly there will be a resonance tail into the low energy region, combined with strength from higher p-wave states; no radiative width is known for this state. The situation is similar for a possible 2^+ state at $E_x = 11.16$ MeV in ^{12}C with a width of $\Gamma = 430$ keV. There is also the possibility of direct capture from the d wave into the ground state of ^{12}C. Somewhat different is the situation for the f-wave state at 9.641 MeV, $\Gamma = 34$ keV, where both the radiative and particle decay properties are known. This state has been included as a narrow resonance in stellar rate compilations. However, the tail of this resonance should be included more properly in reaction rate calculations.

2.3. The stellar reaction rate of the triple-α reaction

In Ref. [10] the question of the stellar rate of the triple α reaction for very low temperatures has been raised. It has been argued that in this case the population of the ground state of ^{8}Be is not in thermal equilibrium with its environment, i.e., the number of ^{8}Be atoms is not given by the simple narrow state formalism.[5] Rather a full stellar reaction rate integral for the low energy tail of the ^{8}Be ground state was performed and was multiplied by the $^8\mathrm{Be} + \alpha$ stellar reaction rate. In both reaction rate cases simple single-state Breit–Wigner forms were used for the cross section dependence in the reaction rate integral. As mentioned above, some pieces of the cross section are thus definitely missing.

While such an approach may be justified for low temperatures (given the levels of our ignorance and the particular degree of desire to know it more precisely), for high temperatures both a description of the 0^+ strength in ^{8}Be as well as the population of the broad $E_x = 3$ MeV 2^+ state in ^{8}Be ($\Gamma = 1.5$ MeV) have to be taken into account. This has not yet been done. In addition, the cross section of the $^8\mathrm{Be} + \alpha$ reaction, as discussed above for high temperatures, has to be treated more adequately than has been done previously. The determination of the triple-α reaction rate at temperatures far above, and below those for normal hydrostatic helium burning therefore remain formidable problems, mainly because obtaining the needed experimental information about the location, particle widths and γ-widths of any relevant state of ^{12}C, or the strength of direct processes, appears to be very difficult.

3. The ^{12}C(α, γ)^{16}O reaction

3.1. General situation

The stellar rate of hydrostatic helium burning for the $^{12}\mathrm{C}(\alpha, \gamma)^{16}\mathrm{O}$ reaction remains one of the most important unsettled rates left in Nuclear Astrophysics. Its special importance

[5] In the narrow state limit the population is independent of the life time or width of the narrow state.

to stellar modeling arises from the fact that the $^{12}C(\alpha,\gamma)^{16}O$ reaction in the helium core of a star takes place simultaneously with the triple α reaction (see Section 2). For a given thermal environment, the ratio of these two reaction rates is fixed in contrast to the burning stages of a star where the flow through only one reaction at a time is important. Such single reaction flow can then be easily adjusted by minor changes, e.g., in temperature arising from a change in model or reaction rate. In contrast, the ratio of carbon and oxygen at the end of the helium burning phase of stellar evolution is given by the ratio of the stellar reaction rates of radiative α capture on ^{8}Be and ^{12}C. Variations in these ratios for stars of different masses lead then to quite different developmental paths and final element production ratios.

The difficulty in experimentally determining the rate of $^{12}C(\alpha,\gamma)^{16}O$ for quiescent helium burning, which typically takes place around center-of-mass-energies of 300 keV in the $\alpha + {}^{12}C$ system, arises from the fact that the cross section is very small ($\approx 10^{-17}$ b) and far beyond direct measurements in the foreseeable future. The extrapolation to low energies is difficult as the cross section in this energy region is a mixture of groundstate and cascade transitions with no state of natural parity in ^{16}O available for radiative capture near 300 keV energy. The cross section for the ground state transitions is indeed dominated in this energy region by the tails of subthreshold resonances with other processes interfering. Cascade transitions, expected to be smaller in cross section, are often dominated by direct processes, but subthreshold state influences are possible. In Fig. 1 relevant states for the $^{12}C(\alpha,\gamma)^{16}O$ problem are shown.

While radiative widths of states in ^{16}O are often well known, it is in general the α-widths of states, in particular those below the $^{12}C + \alpha$ threshold, that cause the problems in predicting the stellar rates of $^{12}C(\alpha,\gamma)^{16}O$ at low energies. These α widths can be inferred, however, by indirect methods like the β-delayed α decay of ^{16}N, elastic scattering, or direct radiative capture. However, even if the knowledge of the α widths were complete, the interference signs between different components of the cross section need to be derived from direct measurements.

For ground state transitions both E1 and E2 capture components are possible. These can be disentangled by γ-angular distributions. Many of the published papers have carried out this step in the data reduction. For cascade transitions there are in principle four independent cross sections to be extrapolated to 300 keV, namely those for transitions to the 6.0 MeV (0^+), 6.1 MeV (3^-), 6.9 (2^+) and 7.1 (1^-) excited states in ^{16}O. These four cross sections each have their own problems in extrapolation, as complicated as those for the ground state transitions, but most likely have smaller cross sections at helium burning temperatures than the ground state transitions.

3.1.1. Theoretical considerations

There have been several approaches to the problem of extrapolating the $^{12}C(\alpha,\gamma)^{16}O$ cross section to the relevant low energies. These can be roughly classified as model based and phenomenologically based. The first class would comprise potential and cluster models, while the second class would include R or K matrix parameterizations, and some even simpler approaches. The model based extrapolations predict the cross section based on the fitting of a few general nuclear parameters, though in many cases they will require scaling to actual cross section at higher energies. R and K matrix ap-

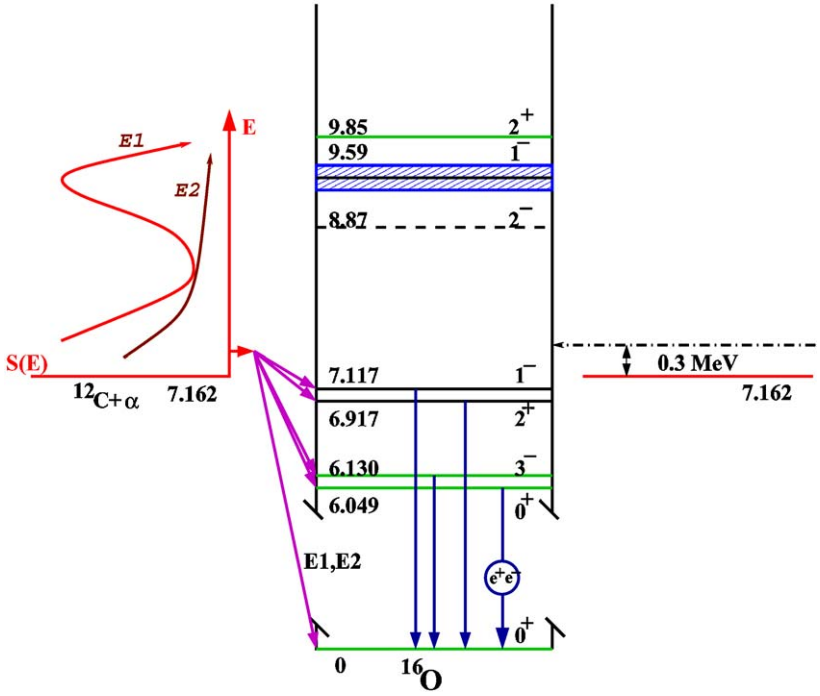

Fig. 1. ^{16}O states relevant to the ^{12}C$(\alpha, \gamma)^{16}$O reaction.

proaches on the other hand rely on the fitting of as many data as possible, to restrict the many parameters per state (up to four in a single channel description) as much as possible. Somewhere between is the hybrid R-matrix approach in which one state may be modeled in a potential model, while other states use R-matrix parametrization. In general, model based predictions do not predict all the data, but normally a rather limited set and show little flexibility to allow a reasonable error estimate. We will therefore largely use the R-matrix approach as described in Ref. [11]. In R (and K) matrix theory the α elastic channel is the only open channel below the $\alpha + {}^{12}$C first-excited-state (4.44 MeV) threshold; the γ-decay from excited states of ^{16}O and β decay to these states can be treated as perturbations. Both elastic scattering and the data from the β-delayed α-decay of ^{16}N can therefore be incorporated into the analysis, in straightforward ways.

In the following, we will describe the measurements, data and fits of the usual ingredients into the extrapolation of the ^{12}C$(\alpha, \gamma)^{16}$O reaction cross section, i.e., elastic scattering data and the β-delayed α-decay spectrum of ^{16}N. We will then discuss the present radiative capture data, and what can be learned with all data combined. This will apply to both the ground state and cascade data. At the end, we examine, how the extrapolation of the total ^{12}C$(\alpha, \gamma)^{16}$O reaction cross section can possibly be improved and present a discussion of the derivation of the stellar reaction rate.

3.2. $^{12}C + \alpha$ elastic scattering

Elastic scattering data of α-particles on ^{12}C have been used for a long time in the extrapolation of the $^{12}C(\alpha,\gamma)^{16}O$ reaction cross section. The reason is that these data contain the α particle information for all relevant states in ^{16}O and can be obtained with rather high accuracy, if sufficient care is taken. Also, α-partial wave information is needed for phase information in the analysis of γ-ray angular distributions.

Several measurements [12–25] of $^{12}C(\alpha,\alpha)^{12}C$ have been made as early as 1953. While there have been some elastic data taken with a carbon beam on a helium gas target in the context of radiative capture measurements, all of the explicit elastic scattering measurements employed α (helium) beams on thin carbon foils and measured scattered α angular distributions. The numbers of angles measured varies from two to 32; different angles were determined sometimes by rotating the detector table, or by providing a large number of fixed detectors. A typical experiment is described in [25]. Normally the scattering data have then undergone phase shift analysis and only the derived phase shifts have been published, sometimes without error bars. Only a few measurements have provided phase shift error bars [20,23], and only one [23] has made the primary data available [25,26]. While phaseshift analyses are preferred in theoretical modeling (like potential models) as they separate states and partial waves of different spins, there are inherent problems connected with the non-linearity of the analysis [27].

It has been discussed in Ref. [27] how the phase shift analysis of $^{12}C + \alpha$ leads to a coupling of partial waves; i.e., resonances of one partial wave are visible as a distortion in other partial waves. Fig. 2 shows a phase shift analysis of the Notre Dame data [25] for $\ell = 1$. Clearly, all $\ell \neq 1$ resonances are visible as distortions in the excitation function. While narrow resonances can easily be removed in a fit, it is not clear, whether there is an underlying influence of background states or wide resonances of different partial waves. This in principle may distort the results which are sensitive to these properties. Therefore a global analysis of elastic data was proposed, i.e., taking all angular momenta into account simultaneously.

3.2.1. Global analysis of Notre Dame data

Ref. [25] describes an elastic $^{12}C + \alpha$ scattering experiment in which a global R-matrix analysis has been employed. The following conclusions were drawn: the best fit for the reduced width amplitude[6] of the 2^+ subthreshold state ($E_x = 6.917$ MeV[7], $E = -245$ keV[8]) occurred for $\gamma_{12} = 0.47$ MeV$^{1/2}$, with $\gamma_{11} = 0.27$ MeV$^{1/2}$ for the

[6] For R-matrix notation, see Refs. [27,28], references therein, and footnotes in Section 3.5.1. The reduced width amplitude γ_{12} is a measure of the α width of a state. The indices 12 indicate the first state of angular momentum two, i.e., the 6.9 MeV state in ^{16}O. S(300) of the ground state transition scales approximately with the square of the reduced width amplitude.

[7] For conciseness in the subsequent text, state energies will be truncated to two significant figures and may be used as indices for symbols, e.g., $\theta_\alpha^{6.9}$.

[8] 'E' labels the center-of-mass energy in any system discussed in this article.

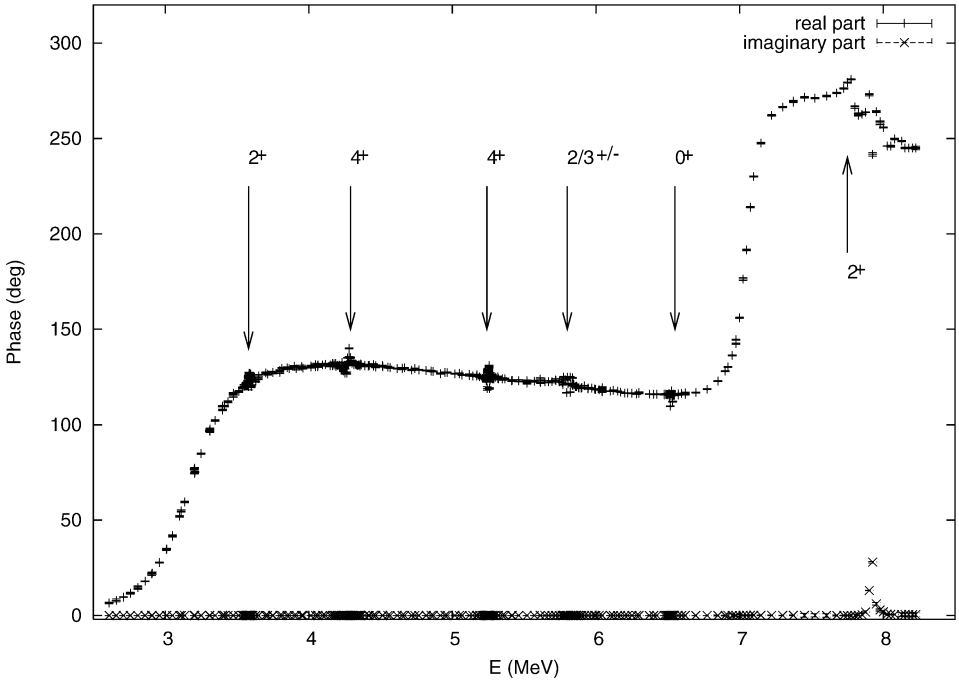

Fig. 2. $\ell = 1$ phase shift data for the Notre Dame experiment [25], showing both the real and imaginary phases as well the positions of $\ell \neq 1$ resonances.

subthreshold 1^- state ($a = 5.5$ fm). To derive an error estimate, fits were obtained for values of γ_{12} from 0.2 to 0.60 MeV$^{1/2}$, with all other parameters allowed to vary. The same approach was used to scan γ_{11} from 0 to 0.60 MeV$^{1/2}$ for the 1^- state. 1σ uncertainties of $\gamma_{12} = 0.47 \pm 0.06$ MeV$^{1/2}$, and $\gamma_{11} = 0.27^{+0.11}_{-0.27}$ MeV$^{1/2}$ were calculated with the previously established [28] guideline $\chi^2 < \chi^2_{\min} \pm 9\chi^2_\nu$. This has to be compared to $\gamma_{11} = 0.18 \pm 0.02$ MeV$^{1/2}$ of Ref. [28]. The best fit has a χ^2_ν of approximately 1.66. Deviations from an ideal fit occurred at resonances with widths in the keV range where the sensitivity to target effects and beam energy calibration would be most pronounced.

The influence of the interaction radius[9] a on the results was also investigated in Ref. [25] using elastic scattering data. A strong dependence of the least-squares parameter χ^2 as a function of a was found in the Notre Dame data with $a = 5.42^{+0.16}_{-0.27}$ fm as the best value. The width γ_{12} decreases, as expected, with increasing a. Close to the minimum, an approximate $1/a$ dependence is found for γ_{12} and other widths. This result justifies using $a = 5.5$ fm throughout the discussions below and represents the first real restriction on the interaction radius a in the $^{12}\mathrm{C}(\alpha,\gamma)^{16}\mathrm{O}$ problem.

[9] The interaction radius a is the size of the square potential in R-matrix theory. It is, in principle, a free parameter though somewhat constrained by nuclear theory (and reason).

3.3. The ^{16}N β-delayed α-spectrum

3.3.1. General information

The β-decay of ^{16}N populates the ground state and excited states in ^{16}O, some of them above the $^{12}C + \alpha$ threshold at 7.162 MeV. As the ^{16}N ground state spin and parity are $J^\pi = 2^-$, states with 1^-, 2^-, and 3^- spin and parity are populated in allowed Gamow–Teller transitions. α-decay can only occur with a significant probability from states with natural parity. Thus the α-decay properties of $J^\pi = 1^-$ and 3^- states are probed by the β-delayed α-decay of ^{16}N. The β-decay itself can be treated as a perturbation not influencing the wavefunction of the ^{16}O compound state, thus resulting in a simple energy-dependent function (Fermi function) times a scaling amplitude (feeding factor) in the R- or K-matrix description of the β-delayed α-spectrum of ^{16}N.

The 1^- amplitude in the α energy range covered by the β-decay of ^{16}N is dominated by the 9.59 MeV 1^- state in ^{16}O. However, this amplitude interferes with the one from the 7.12 MeV 1^- state below threshold and possible contributions from higher lying states. In the β-decay of ^{16}N the 9.6 MeV state is populated at about 1×10^{-5} while the 7.1 MeV state is populated at 5%. This amplifies the influence of the subthreshold state in the β-delayed α-spectrum of ^{16}N. For the 3^- amplitude there is no state within the α-energy window presented to the β-decay; thus only a far away subthreshold state and higher energy amplitudes contribute.

Experimentally, the small β branching ratio into α-decaying states of ^{16}O combined with the fact that the low energy side of the spectrum is of particular importance provides some formidable challenges. For one, a high yield of ^{16}N is required. Furthermore, any possible detector should be as insensitive as possible to the high β-particle flux. In addition, high-energy α-particles can be degraded (scattered) both in the source as well as in the detector, reducing α-particles to lower energies and distorting the spectral shape.

3.3.2. Measurements

3.3.2.1. The Wäffler spectrum Three publications spanning the period 1969–1974 [29–31] describe a successful search for the parity-forbidden α-decay of the $J^\pi = 2^-$ 8.87 MeV state of ^{16}O, carried out at the Max-Planck-Institut für Chemie, Mainz, Germany. The technique chosen was to examine carefully the β-delayed α spectrum from the β-decay of ^{16}N to various excited states of ^{16}O by accumulating very large numbers of α-particles to achieve a smooth spectrum with very small statistical fluctuations in each energy channel in the spectrum. While the first publication from the experiment was not able to isolate a weak α group corresponding to the 2^- state, it did identify a group corresponding to the 2^+, 9.84 MeV state of ^{16}O, following a first-forbidden β-decay branch of the ^{16}N decay. Eventually, with a still larger number of α-particles, the experiment was successful in finding an even weaker group corresponding to the parity-forbidden α-decay of the 2^- state at 8.87 MeV, an achievement not duplicated to this date. However, as there is no experimental correction for detector and target response, the Mainz data cannot be used in fits to other data, as we will argue below.

The three papers describe the details of the experiment well, including the amount of absorbing material external to the silicon surface barrier α detectors, thus allowing one to evaluate the (α-energy-dependent) energy losses by the α-particles before they enter the sensitive volume of the detectors.

In 1971, Prof. H. Wäffler sent lists of approximately one quarter of the data obtained for the 1970 Phys. Rev. Lett. paper [30], to Barnes and Barker, together with a very precise calibration for the energy spectrum as measured within the α-detectors (10.60 keV per channel) [32]. For brevity, this spectrum will be referred to as the *Mainz 71 spectrum*. With this calibration, and the calculated α-energy-dependent energy loss in the absorbing layers, the Mainz 71 spectrum can be corrected to the energies with which the α particles were emitted from the ^{16}O breakup. The location of the spectrum on the energy scale is firmly established by Prof. Wäffler's identification of the channel where the α-particles from the 2^- state (now know to be at $E_\alpha = 1282 \pm 0.5$ keV) were to be expected, and the channel where the α-particles from the 2^+ state (from the ^{16}N first forbidden decay) were found (now known to be at $E_\alpha = 2011 \pm 0.6$ keV) [33].

Over the limited energy range of the Mainz 71 spectrum, from ~ 1.1 MeV to ~ 2.1 MeV, the correction for the energy absorbed by the overlying layers is very nearly a linear function of the energy because of the nature of the energy loss before the α-particles reach the detector sensitive volume. In fact a straight line calibration between these two fixed points, the 2^- and 2^+ states, differs by no more than 1 keV from the detailed calibration.

It may seem that understanding the calibration of the Mainz 71 spectrum is a mere technical detail. However, it becomes important when comparing the Mainz 71 spectrum and the β-delayed α-spectra of the experiments discussed below (Sections 3.3.2.2 and 3.3.2.3). The interpretation of the meaning of the Mainz 71 spectrum calibration presented above was verified by Prof. Wäffler in a private communication [34].

3.3.2.2. The Yale/University of Connecticut data About 25 years later, concurrent independent measurements of the β-delayed α-spectrum from the ^{16}N β-decay were carried out by groups at Yale University, and at the TRIUMF Laboratory, to explore the suggestion of Ref. [35] that this experiment could help in determining the E1 astrophysical S-factor for $^{12}\mathrm{C}(\alpha, \gamma)^{16}\mathrm{O}$. The measurement of the β-delayed α-spectrum of ^{16}N done at Yale University is described in Zhao et al. [36]. In their experiment, a ^{15}N beam impinged on a deuterated target. A small fraction of the recoiling ^{16}N atoms from the $^{15}\mathrm{N(d, p)}^{16}\mathrm{N}$ reaction was caught in an aluminum stopper foil which was rotated in front of the detection station where the β-delayed α-decay of ^{16}N was recorded. A β–α time of flight apparatus was used. The spectrum, compared to the Mainz (Section 3.3.2.1) and TRIUMF (Section 3.3.2.3) data, was shifted to lower energy, and was considerably broader [37]. A deconvolution described below was then carried out. Later a value of $S_{\mathrm{E1}}(300) = 95$ keV b was derived for the $^{12}\mathrm{C}(\alpha, \gamma)^{16}\mathrm{O}$ reaction using the R-matrix parametrization of [35].

It is clear from an examination of [36] and [37] that the two step "unfolding" of the data for $1.0 \leqslant E_\alpha \leqslant 2.5$ MeV is essentially an energy-dependent normalization of the energy-shifted raw experimental α-spectrum [36, Fig. 1(a)] to agree with the high statistics Mainz 71 spectrum of Refs. [30,32]. There is no explicit statement [36,37] concerning

the "unfolding" process in the energy region $E_\alpha \leqslant 1.0$ MeV. However, it was stated [38] that the "unfolding" here was guided by a theoretical curve of Ref. [35] (with the best fit corresponding to $S_{\mathrm{E1}}(300) = 90$ keV b). It appears, therefore that a similar normalization was employed for the data in the range $E_\alpha \leqslant 1$ MeV. By following these procedures it is straightforward to recreate the final unfolded spectrum of [36]. It is thus reasonable that the subsequent R-matrix analysis of the "unfolded" spectrum should yield a result near 90 keV b [35].

With regard to the R-matrix fit, it has been shown in [28,39] that it is necessary to do a complete $\ell = 1$ and $\ell = 3$ fit to the data, along with the incorporation of appropriate background parameters. In the analysis of [36], the $\ell = 3$ component was an arbitrary function imposed by the authors on their fitting procedure as a precondition (labeled "fit" in [36], but called "ad hoc" in [37]). To justify this procedure it was argued [36] that any f-wave can only influence the final S-factor by 15%. This argument is not correct for it is easy to obtain many different f-waves, some that even follow approximately the shape of the low energy interference anomaly of the α-particle spectrum (a case that can be excluded only by a spectrum with good statistics [28]). From Refs. [36,37] there is also no evidence that a least-squares fit has been carried out, but rather that the theoretical curves from [35], used in the normalization of the "raw" spectrum were also used as templates to obtain the best comparison of one of them to the data.

A further measurement by the Yale/University of Connecticut group was reported in the conference proceedings of Nuclei in the Cosmos IV [40]. In addition, a ^{16}N β-delayed α spectrum by a Seattle group is shown in [40]; to this date this measurement has not been published. While little information is given in Ref. [40] about the Yale experiment, a thesis describing this experiment is available [41]. With a similar setup to Refs. [36,37], considerably more counts of β-delayed α particles were detected. The spectrum shows a similar energy shift and broadening to the one in Refs. [36,37]. For these results, deconvolution of the experimental β-delayed ^{16}N α spectrum was carried out by dividing the spectrum by the resolution function.[10] The resultant spectrum thus derived was then compared with other spectra [41] with the conclusion that the TRIUMF α spectrum [28] (Section 3.3.2.3) shows a narrower main peak than the others. No S-factor for the ground state E1 transition was derived [41].

The methods used for deconvolution of the raw experimental α spectra data in Refs. [36, 37,40,41] are both inadequately explained and justified, while the R-matrix fitting procedures are unclear. In addition, the authors of Refs. [36,37,40,41] actually disagree with the Mainz 71 spectrum, contrary to their claims, because they have incorrectly interpreted the pulse height calibration given by Wäffler along with the Mainz 71 spectrum (Section 3.3.2.1) to obtain an α -spectrum which they then compare to the TRIUMF data [28]. In their comparison the Yale/Connecticut group uses a constant energy/channel dispersion without energy loss corrections, to calibrate their Mainz 71 spectrum, thus ignoring energy-dependent energy losses described above (Section 3.3.2.1). Over the ~ 1 MeV energy range of the Mainz 71 spectrum, the external energy loss changes from about 75 to

[10] The energy dependent resolution was measured by using the width of the β-delayed α-spectrum of ^{8}Li without considering β–α recoil broadening.

57 keV, changing the energy per channel by an order of magnitude more than implied by the precision of the value given by Wäffler [31,34]. In addition, the large energy resolution (200 keV quoted in Ref. [40]; up to 400 keV quoted in Ref. [36]) necessitates large (energy dependent) renormalizations. For these reasons, we have not included the Yale/Connecticut data in our least squares fits to obtain $S_{E1}(300)$.

3.3.2.3. The TRIUMF data A measurement of the β-delayed α spectrum of ^{16}N has been reported in Ref. [28] totaling more than 1 million events. The measurement was done using a mass-separated low-energy ^{16}N beam, from the isotope separator TISOL, which was implanted into a very thin (10 $\mu g/cm^2$) carbon foil. The foil was then rotated to a position between two thin silicon surface barrier detectors. In these opposite detectors both the α particle and the recoiling ^{12}C nucleus were detected in coincidence.

The energy calibration scales of the α-detectors were determined directly from the β-delayed α-groups from the decays of ^{18}N and ^{20}Na in the identical apparatus used for the study of the ^{16}N β-delayed α-spectrum. When the spectrum from the TRIUMF experiment was compared with that of the (fully calibrated) Mainz 71 spectrum, we found that the two spectra agreed very well over and above the main peak, while the Mainz 71 spectrum was slightly wider than the TRIUMF *coincidence* spectrum on the low energy side of the main peak. This low energy broadening of the main peak of the Mainz 71 spectrum is no doubt caused by some α-particle energy degradation in the absorbing layers. Fig. 3 shows the

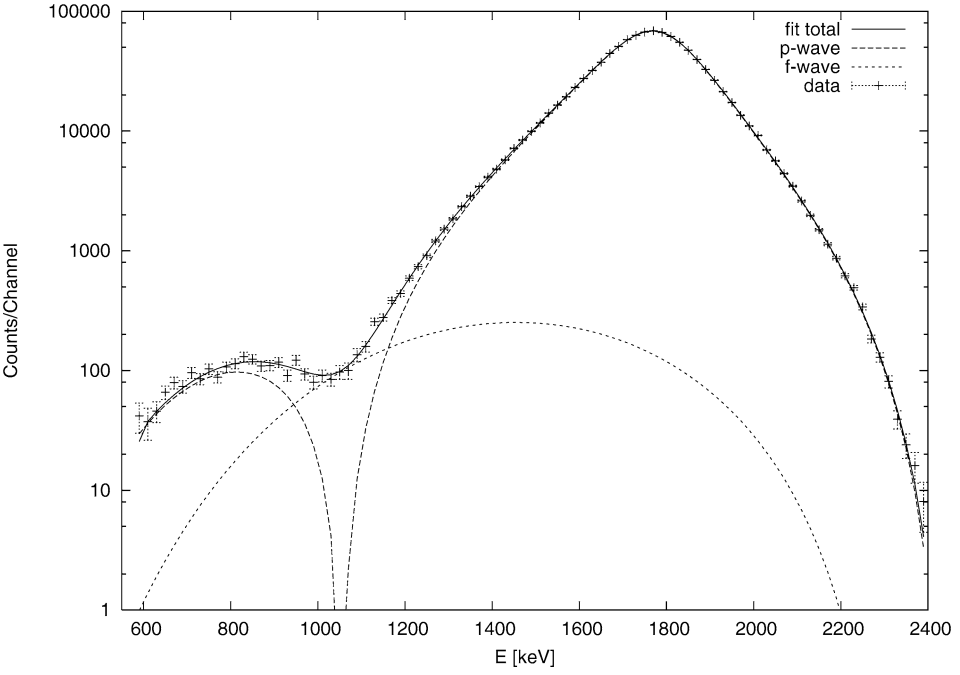

Fig. 3. The TRIUMF coincidence spectrum of β-delayed α-particles from the decay of ^{16}N. The x-axis displays the laboratory α-energy. In addition, an R-matrix fit to the data is shown, including the p- and f-wave components.

TRIUMF coincidence spectrum. It may be noted that the data point at 2010.1 keV (not included in the fit) is 3.4σ above the R-matrix fit to the other data, and corresponds to the position of the 2^+ state.

The energy of the breakup of the ^{16}O nuclei that result from the ^{16}N β-decay is shared between the α- particles and their ^{12}C recoils in the ratio of 3 : 1. Thus, in the two-dimensional coincidence spectra from the TRIUMF experiment, the locus of related α-particles and recoil ions is easily visible, and energy degraded events can be clearly identified and removed from the α-spectra. Thus the coincidence α-spectrum is also slightly narrower on the low energy side of the main peak than the single event-detector spectrum.

The interference between the α-particles from the high-energy tail of the subthreshold 7.1 MeV state and the 9.6 MeV state is clearly visible in the low energy region of the TRIUMF α-spectrum. R-matrix analysis of the α-spectrum together with existing radiative capture data and elastic scattering data led to $S_{\mathrm{E1}}(300) = 79 \pm 21$ keV b. As will be shown later in our analysis, this value can be still used unchanged to this date.

3.3.3. Complex feeding factors

In Ref. [42] it was proposed to use a complex β-decay feeding factor to the $E_x = 9.6$ MeV state of ^{16}O instead of employing an f-wave contribution to fit the β-delayed α-spectrum of ^{16}N. Such a fit was presented in Fig. 2 of [42]. It was concluded from that fit that the ^{16}N α-spectrum is compatible with a very small E1 ground state S-factor. However, the fit of Fig. 2 shows that no least squares procedure was followed, but rather a fit, by eye, with a high χ^2 was chosen. By introducing a complex feeding amplitude to the $E_x = 9.6$ MeV state of ^{16}O, and minimizing correctly, we find $S_{\mathrm{E1}}(300) = 74$ keV b, in agreement well within errors with 79 keV b [28], when an f-wave was employed. Thus the two ways of fitting seem to be roughly equivalent, though there can be little physical justification to exclude an f-wave contribution to the β-delayed α spectrum of ^{16}N.

3.4. Direct ^{12}C$(\alpha, \gamma)^{16}$O measurements

While there were a few experiments earlier, the 1974 measurement [43] of Dyer and Barnes of the ^{12}C$(\alpha, \gamma)^{16}$O ground state E1 reaction cross section may be the first which led to serious work in understanding the reaction mechanism. Dyer and Barnes used a pulsed α beam on a ^{12}C target, with the detector for most of the measurements at 90°, and at 10 cm distance to allow neutron-γ time of flight discrimination. Four angular distributions were also recorded. The measurements extend from 1.41 to 2.94 MeV and, because of the geometry of the setup, comprise largely E1 ground state data. The small beam (0.3 μA time-averaged) and the residual ^{13}C content of the target precluded measurements at lower energies.

There are additional ground state transition measurements at higher energies. In particular, that of Ophel et al. [44], determined the E1 cross section from 6.5 to 8.5 MeV in a 90° measurement. The E1 strength in this region interferes directly with the $E_x = 9.6$ MeV 1^- resonance below. Additional measurements in this high energy region are quoted in [44].

A measurement in inverted kinematics (with a ^{12}C beam on a helium gas target) was published by Kettner et al. [45] in 1982. It produced ground state and cascade excitation functions ranging from 1.34 to 3.38 MeV. Two NaI detectors in close geometry to a windowless gas target were employed. Data for both the total ground state cross section as well as for cascades (6.9 and 7.1 MeV combined) were derived. The extrapolation used a simplified model, but pointed to the importance of the E2 ground state transition.

A measurement employing an implanted ^{12}C target in gold, an α current approaching 1 mA, and three high resolution germanium detectors, was published by Redder et al. in 1987 [46]. The measurement produced both excitation functions for the groundstate transitions and cascade decay information for the 6.9 and the 7.1 MeV state. The excitation functions range from 0.94 to 2.84 MeV in the center-of-mass. The data were analyzed by an R-matrix analysis.

Kremer et al. [47] report the results of a measurement of $^{12}\mathrm{C}(\alpha,\gamma)^{16}\mathrm{O}$ done with a gas target and a ^{12}C beam employing a γ-detection array and a recoil separator in coincidence. They report E1 ground state data points from 1.29 to 3 MeV which they extrapolate via R-matrix and hybrid-R-matrix. The E1 data were derived by subtracting out the E2 fraction of the yield based on Ref. [46], as the acceptance of the separator did not cover the entire longitudinal phase space at lower energies (see also Section 3.7.1). No cascade data were reported.

Ouellet et al. [48] report a measurement of the $^{12}\mathrm{C}(\alpha,\gamma)^{16}\mathrm{O}$ reaction ranging from 1.37 to 2.98 MeV in nine energy steps. The group employed six germanium detectors at different angles. The targets were ^{12}C implanted in a gold layer. Angular distributions were derived which are available to the public. The fit to the E2 data used a cluster model analysis with only the scale height adjusted.

In 1999, Roters et al. [49] published a measurement of the $^{12}\mathrm{C}(\alpha,\gamma)^{16}\mathrm{O}$ reaction ranging from 0.93 to 3.39 MeV. Absolute values of S_{E1} were given from 1.69 to 3.29 MeV; for the whole energy range, the ratio $\sigma_{\mathrm{E2}}/\sigma_{\mathrm{E1}}$ was given. The method used in the measurement was a ^{12}C beam on a ^{4}He gas target observed by two detectors, one in close geometry, and one far away at 90° (Section 3.5.1). The 90° detector is largely sensitive only to the E1 component of the ground state transition, while the detector in close geometry basically measures the sum of E1 and E2 transitions. A careful analysis of the data then produces the ratio $\sigma_{\mathrm{E2}}/\sigma_{\mathrm{E1}}$. The S_{E1} data agree with previous data; however, the $\sigma_{\mathrm{E2}}/\sigma_{\mathrm{E1}}$ data shown in Fig. 13 of [49] show some problems relative to the fit applied in the high energy region above $E > 2.8$ MeV.

Direct $^{12}\mathrm{C}(\alpha,\gamma)$ radiative capture measurements have been carried out at the Institut für Strahlenphysik of the University of Stuttgart [50,51]. In addition, at the time of preparation of the current review, we became aware of the results of further direct $^{12}\mathrm{C}(\alpha,\gamma)^{16}\mathrm{O}$ γ-ray measurements at the University of Stuttgart over the energy range $0.891 \leqslant E \leqslant 2.8$ MeV [52,53]. These later measurements made use of two different arrays of bismuth–germanate-shielded Ge detectors, and large available α-beam currents up to 500 particle μA. One array consisted of nine detectors covering the angular range from 30° to 130° in each data run; the other array consisted of four detectors, one of which was at a fixed position and the other three could be moved in steps around the target. An R-matrix analysis of the data by this group led to $S_{\mathrm{E1}}(300) = 77 \pm 17$ and $S_{\mathrm{E2}}(300) = 81 \pm 22$ keV b [52].

No direct capture component was included for the E2-radiative capture in the R-matrix treatment [54].

3.5. Data analysis of the radiative capture to the ^{16}O groundstate

3.5.1. Angular distributions

For transitions to the ground state, only E1 and E2 (and higher electric multipole) radiative capture is allowed as only natural parity states can be populated by α-capture on ^{12}C. Only the radiative capture from the p- ($\ell = 1$, E1) and d- ($\ell = 2$, E2) waves are therefore important here for radiative capture into the $J^\pi = 0^+$ ^{16}O ground state. These two transitions mix in the angular distributions[11] following Eq. (1), while they add incoherently in the total cross section. The ways to distinguish E1 and E2 transitions experimentally are either to measure γ angular distributions and evaluate the data by Eq. (1) or, for the E1 transition, to measure at 90° only as the E1 distribution peaks at 90°, while the E2 distribution peaks at 45° and 135°, with no photons being emitted at 90°. With admixtures of E1 and E2 components the distributions are asymmetric with respect to 90°. Note that while the E1 and E2 components for the ground state transition are thus separable, the errors (typically on $S(300)$) derived in fits to these individual components stay correlated in a complicated way which has never been taken into account.

An interesting question is whether there could be an isotropic contribution to the γ radiation, that would somewhat complicate separating the multipoles in the data. In the radiative capture reaction ^{2}H(d, γ)^{4}He, it was found that, at the lowest energies, the gamma ray yield becomes isotropic, apparently because E2 radiation from an incident s-wave ($\ell = 0$) scattering state to a d-state admixture in the ^{4}He ground state dominates the gamma yield curve [55]. However, while it is in principle possible for ^{16}O to have a d-state admixture in its ground state, the spinless nature of ^{4}He, ^{12}C, and ^{16}O makes a similar situation in ^{12}C(α, γ)^{16}O highly unlikely.

[11] The angular radiative distribution for the ground state is an interference pattern between the two electric multipoles E1 and E2, i.e.,

$$W(\theta_\gamma, E) = 1 - Q_2 P_2(\cos\theta_\gamma) + \left[\sigma_{\mathrm{E2}}(E)/\sigma_{\mathrm{E1}}(E)\right]\left[1 + \frac{5}{7} Q_2 P_2(\cos\theta_\gamma) - \frac{12}{7} Q_4 P_4(\cos\theta_\gamma)\right] + \frac{6}{5}\left[5\left[\sigma_{\mathrm{E2}}(E)/\sigma_{\mathrm{E1}}(E)\right]\right]^{1/2} \cos\Phi(E)\left[Q_1 P_1(\cos\theta_\gamma) - Q_3 P_3(\cos\theta_\gamma)\right], \quad (1)$$

where $P_k(\cos\theta_\gamma)$ are the Legendre polynomials, Q_k are the experimental attenuation coefficients of the γ detectors and $\Phi(E)$ is the phase difference between the d and p wave and a Coulomb phase given as

$$\Phi(E) = \delta_2(E) - \delta_1(E) + \arctan\frac{1}{2}\eta \quad (2)$$

with η being the Sommerfeld parameter and δ_i being the nuclear phase shifts. Therefore a fit to a radiative angular distribution in ^{12}C(α, γ)^{16}O is largely sensitive to the ratio of the E1 and E2 cross sections as phase shifts are known from elsewhere (elastic scattering).

3.5.2. The E1 cross section

From E1 data derived this way and fitting simultaneously using Eqs. (3) and (4) for the radiative capture and Eq. (5)[12,13] for the ^{16}N β-delayed α-spectrum one obtains an extrapolation of the cross section to an energy of 300 keV as shown in Fig. 4. The E1 cross section in the low energy region as shown in Fig. 4 is largely the result of the two interfering 1^- states at 7.12 and 9.6 MeV in ^{16}O. For $E \sim 300$ keV the subthreshold 1^- state is dominant. The result of this fit including the β-delayed α-spectrum of ^{16}N is $S_{\mathrm{E1}}(300) = 80 \pm 20$ keV b as in [28].

There has been some discussion about the sign of the interference in the energy region between the 7.1 MeV state and the 9.6 MeV state. The above fit is based on constructive interference between these two states in the low energy region. This seems justified as the combined E1 data available produce a lower least squares fit value for constructive than destructive interference in this energy region. This choice is also supported by the new Stuttgart data. If a destructive fit is forced, the interference minimum is at 3^{+7}_{-3} keV b. Note that, if one considers both destructive and constructive interference possibilities, the allowed region of $S_{\mathrm{E1}}(300)$ is bifurcated but still rather well restricted for either case.

3.5.3. The E2 cross section

Because of the existence of the 1^- resonance state at $E = 2.4$ MeV, the effect of the E2 radiative capture on measurements in this energy region is weak. The cross section in the energy range of the data is a mixture of E2 direct capture and subthreshold resonance capture to the ^{16}O ground state, while the S-factor at 300 keV results mostly from

[12] The E1 data are fitted with

$$\sigma^0_{\mathrm{E1}}(E) = \frac{6\pi}{k^2} P_1(E) \left| \frac{\sum_\lambda \frac{\gamma_\lambda \Gamma^{1/2}_{\lambda\gamma}}{E_\lambda - E}}{1 - (S_1(E) - B_1 + i P_1(E)) R_1(E)} \right|^2 \tag{3}$$

and the energy dependent γ-width

$$\Gamma_{\lambda\gamma} = 2E^3_\gamma \gamma^2_{\lambda\gamma} \tag{4}$$

for the radiative capture and

$$W(E) = f_\beta(E) \sum_{\ell=1,3} P_\ell(E) \left| \frac{\sum_\lambda \frac{A_{\lambda\ell}}{E_{\lambda\ell} - E}}{1 - [S_\ell(E) - B_\ell + i P_\ell(E)] R_\ell} \right|^2 \tag{5}$$

for the ^{16}N β-delayed α-spectrum. Here the index λ indicates summation over states, The index 1 indicating an angular moment of 1, the index γ indicates that the symbol refers to radiative properties. $P(E)$ with an energy indicator refers to the penetrability, $S(E)$ are the shift functions and B the boundary conditions. The R-function is given by

$$R_\ell(E) = \sum_\lambda \frac{\gamma_{\lambda\ell}}{E_{\lambda\ell} - E}. \tag{6}$$

[13] Due to the effective mass for E1 transitions the external parts of the radiative capture cross section are suppressed.

the 6.92 MeV subthreshold state in ^{16}O.[14] Fig. 5 shows the combined data set with the Kunz et al. data [50] added. In addition, we have averaged and rebinned the data every 0.1 MeV. These points are also shown in Fig. 5. There seems to be a clear influence of the $J^\pi = 1^-$ resonance on the data in the $E = 2.4$ MeV region. Again, as in the case of elastic scattering, we attribute this feature to cross-talk of angular momenta in the fits to the angular distributions in this region. In the low energy region there is a gentle slope upward toward low energies, while around $E = 2.6$ MeV the interference pattern from the narrow 2^+ resonance seems to be visible.

[14] For the ground state E2 transition in $^{12}\mathrm{C}(\alpha,\gamma)^{16}\mathrm{O}$

$$\sigma_{\mathrm{E2}}^0 = \frac{5\pi}{k^2}\left|U_0^2(E)\right|^2 \tag{7}$$

with the scattering function

$$U_0^2(E) = -ie^{i\Omega_2}2P_2^{1/2}k_\gamma^{5/2}\left[\sum_{\lambda\mu}\gamma_\lambda^2\gamma_{\mu\gamma 0}^2A_{\lambda\mu}^2 + \frac{3}{\sqrt{10}}\frac{M_n^{1/2}e}{\hbar k}N_f^{1/2}a^2F_2(a)G_2(a)\theta_\alpha^0(2200|00)J_2'(2,0)(E)\right], \tag{8}$$

where the $A_{\lambda\mu}$ are the elements of the state matrix (for more notation see Eq. (14)) [11]. $\Omega_2 = \omega_2 - \phi_2$, ω_2 is the Coulomb phase shift, ϕ_2 the hard sphere phase shift [11], P_{ℓ_i} the penetrability, $k_\gamma = \frac{E_\gamma}{\hbar c}$ the radiative wave number, M_n the atomic mass unit, e_q the electric unit charge, and $F_{\ell_i}(a)$ and $G_{\ell_i}(a)$ the regular and irregular Coulomb functions at the radius a, respectively. Therein is M_n the atomic mass unit (931 MeV/c^2). From the normalization of the wave functions,

$$N_f^{-1} = 1 + \frac{2(\theta^0)^2}{a}\int_a^\infty dr\left[\frac{W_0(r)}{W_0(a)}\right]^2 \tag{9}$$

with the dimensionless reduced width amplitude for the α-particle

$$\theta_\alpha^0 = \gamma^0\left(\hbar^2/\mu a\right)^{-1/2}. \tag{10}$$

$W_J(r)$ are the Whittaker functions, i.e., to a very good approximation the continuation of the bound state wavefunction outside the channel radius a. In similar fashion

$$J_2'(2,0)(E) = \frac{1}{a^3}\int_a^\infty dr\, r^2\frac{W_0(r)}{W_0(a)}\left[\frac{F_2(r)}{F_2(a)} - \frac{G_2(r)}{G_2(a)}\right]. \tag{11}$$

Note the overlap between the Whittaker ground state function (index 0) and the Coulomb scatter functions (index 2) in the integral $J_2'(2,0)$.

The γ-width $\gamma_{\mu\gamma 0}^2$ can in principle be divided into internal and external regions

$$\gamma_{\mu\gamma 0}^2 = \gamma_{\mu\gamma 0}^2(\mathrm{int}) + \gamma_{\mu\gamma 0}^2(\mathrm{chan}), \tag{12}$$

with the internal part normally dominant and the channel part given by a similar expression to the direct one, i.e., the right part of the sum in Eq. (8) [11].

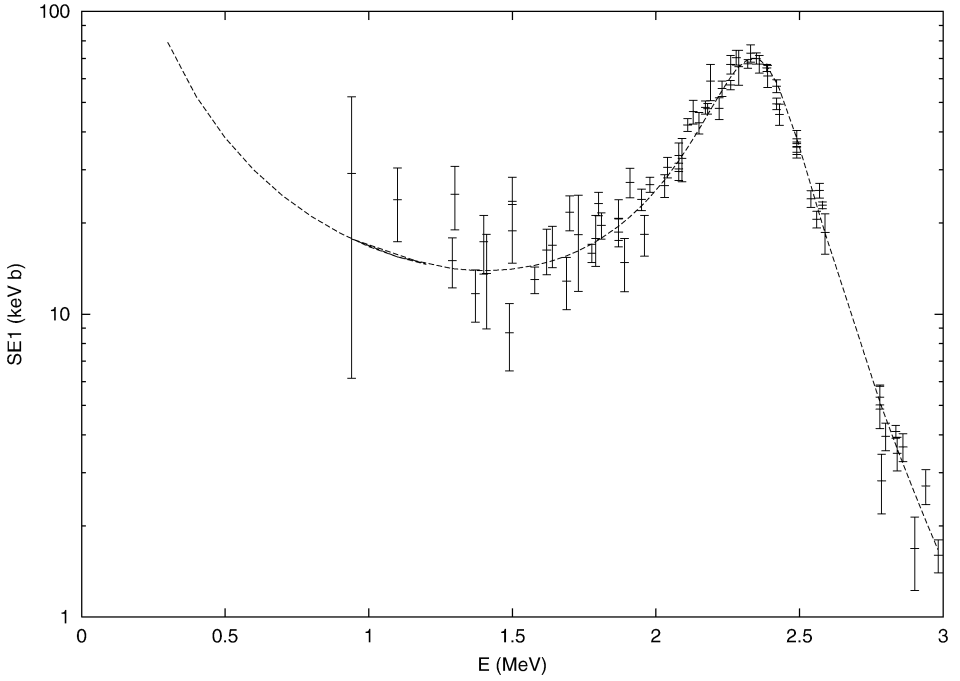

Fig. 4. The E1 S-factor of $^{12}C(\alpha,\gamma)^{16}O$ obtained in a simultaneous fit to the ^{16}N α spectrum, and the radiative capture cross sections.

Previous extrapolations of $S_{E2}(300)$ have been made using simultaneous fits to all available primary data [27]. Direct inclusion of all of the elastic scattering data discussed above (Section 3.2.1 [25]) will, however, statistically dominate other data sets. For this reason, the reduced width amplitude γ_{12} can be directly fixed within its errors in such fits without significantly narrowing the χ^2 range estimated in the minimization. Therefore the best-fit elastic scattering parameters for the 2^+ states can be combined with radiative capture data [43,46–49] from $^{12}C(\alpha,\gamma)^{16}O$ and ^{16}N data [28]. This analysis carried out in Ref. [25] leads to a value of $S_{E2}(300) = 49^{+7}_{-9}$ or 58^{+8}_{-11} keV b, depending on the sign of the $E = 4.36$ MeV 2^+ resonance γ width amplitude relative to that for direct capture and the subthreshold resonance. As this interference sign is unknown, the two results are averaged and errors include the limits on both measurements, yielding $S_{E2}(300) = 53 \pm 13$ keV b. With the full range of a allowed by the Notre Dame elastic scattering experiment, the final result is $S_{E2}(300) = 53^{+13}_{-18}$ keV b [25]. In this analysis destructive interference between the ground state direct capture and the tail of the subthreshold 2^+ resonance has been employed. This is justified by a total decrease in χ^2 of nearly 300 between the destructive and constructive options resulting largely from the γ-angular distributions of Refs. [46,48] and the E2 data in Fig. 5. However, additional angular distributions of the ground state at both low and higher energies are desirable, as the constructive option leads to 92 or 102 keV b, respectively, for $S_{E2}(300)$. At this time we do not have the detailed Stuttgart data needed to include those data in our χ^2 minimization.

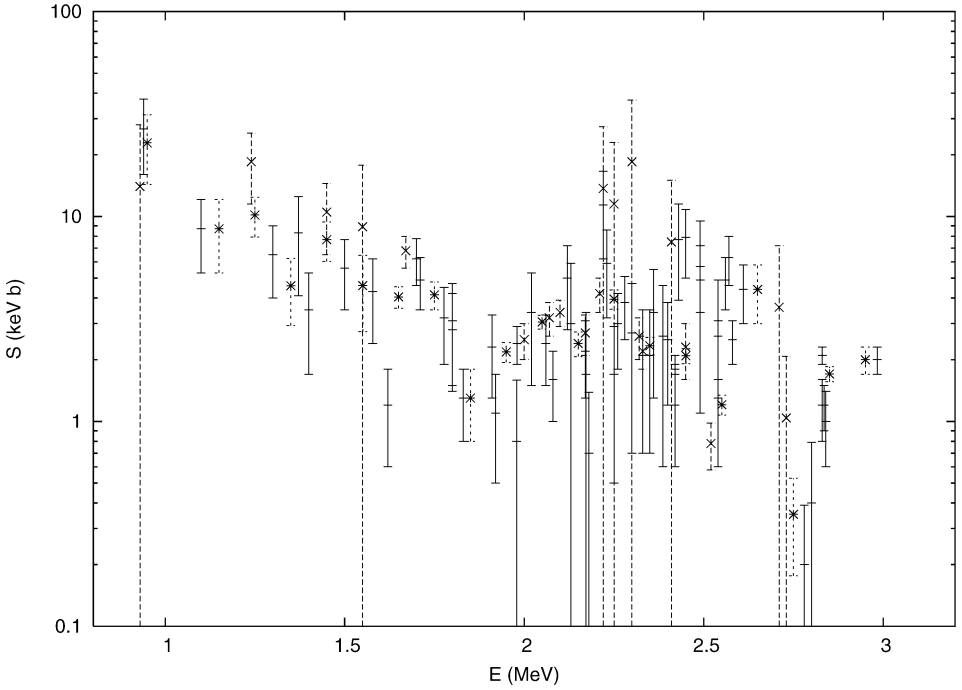

Fig. 5. The E2 S-factor of $^{12}C(\alpha,\gamma)^{16}O$ ground state transition. Bar, previous data; cross, Kunz et al. data [50]; star, averaged and rebinned data.

3.6. Cascade transitions

Cascade transitions, i.e., capture to excited states of ^{16}O below the $^{12}C + \alpha$ threshold, have in general lower cross sections than the ground state transition. Therefore relatively little attention has been paid to determine their strengths. However, all the features of the ground state transition repeat themselves in the cascade cross sections. That is, interfering resonances, subthreshold states, and direct processes are necessary to fully describe these cross sections.

It should also be noted that the 6.0 (0^+), 6.9 (2^+) and 10.3 (4^+) MeV states may form a rotational band in ^{16}O [57]. This implies that their internal structure, i.e., their reduced α-width θ_α should be about the same. Since we know the width of the unbound 10.3 MeV state very well, there is only a limited range of values for the reduced α-width of the 6.9 MeV state (Eq. (10)).

3.6.1. Capture to the 6.0 MeV state

Capture to the 6.0 MeV (0^+) state of ^{16}O is thus far unobserved, except for the decay of two 2^+ resonances. The reason is, of course, that there is no high energy secondary γ decay of this state, while the primary γ emission with energies of 2–4 MeV tends to be overwhelmed by background events in typical γ-ray detectors. This is not a concern with a recoil separator (see Section 3.7.1). DRAGON has indeed observed this transition above

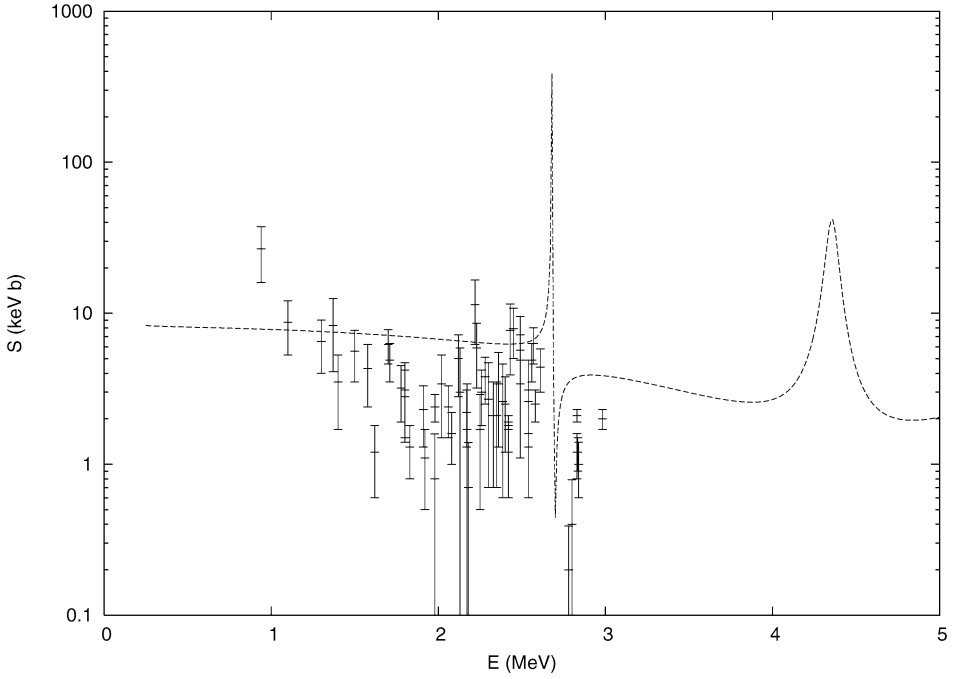

Fig. 6. The E2 S-factor of the $^{12}C(\alpha, \gamma)^{16}O$ transition to the 6.05 MeV state (dashed curve). For comparison, the E2 ground state data are also shown.

$E = 3.1$ MeV, exceeding the ground state transition strength in this energy region. Fig. 6 shows a possible energy dependence of such a transition based on preliminary DRAGON data and the known branching ratios in the 2^+ resonances. In principle this transition should show similar behaviour to the ground state transition, i.e., 1^- and 2^+ states should be involved, including direct contributions for E2 transitions. However, for the $E_x = 7.1$ and 9.6 MeV 1^- states, no transition to the 6.0 state has been found. For the 2^+ resonance in the energy region transitions are known; however, the $6.9 \rightarrow 6.0$ transition is very weak. Therefore subthreshold state contributions are not expected to be important. As only the E2 component has known resonance contributions and a possible direct component, this part of the cross section is most likely the larger part of the 6.0 cascade cross section and is shown in Fig. 6, assuming a larger cross section above $E = 3.1$ MeV than the ground state transition. This can only be achieved by adjusting the direct E2 component, which as Fig. 6 shows is also dominant at $E = 300$ keV; resonances do not matter much. The cascade transition to the 6.0 MeV state can therefore be estimated to be a few keV b at $E = 300$ keV, pending further data.

3.6.2. Capture to the 6.9 MeV state

The capture to the 6.9 MeV state has both resonant and direct components. E2 direct capture from the $\ell = 0$, 2, and 4 partial waves is possible. States with $J^\pi = 0^+$, 2^+, and 4^+ will interfere with the direct capture process in the total cross section, while resonances with different J^π will add incoherently. Resonances up to the proton threshold have been

included in the calculation to follow; however, there is no radiative capture information available for the 3^- state at $E = 4.42$ MeV and the 0^+ state at $E = 4.89$ MeV [56]; in order to estimate their effects some γ-cascade strength has been assumed for these states. Existing cascade data [45,46] cover a range from $E = 1.4$ to 3.225 MeV where both of these states of unknown radiative decay strength are unimportant. We note a slight discrepancy between the data of Kettner et al. [45] and Redder et al. [46] in the 1^- resonance region, as the Kettner data (obtained with a NaI detector) should include transitions to both the 6.9 and 7.1 MeV states, while Redder et al. separated those with a germanium detector. However, the S-factor of Kettner et al. and of Redder et al.'s 6.9 MeV transition agree very well, but the sum of the 6.9 and 7.1 MeV transitions in Redder et al. exceeds by far Kettner et al.'s data.

The data include the 2.43 MeV 1^- resonance, the 2.68 MeV 2^+ resonance (though data are not published on top of it) and the 3.20 MeV 4^+ resonance [56]. The γ-strength for the 1^- and 4^+ states can be fitted to the data. Other γ-strengths are taken from Ref. [56]; the lower 4^+ resonance has the largest cascade cross section because the 6.9 MeV cascade transition is the most likely γ-decay branch, while for the other resonances this branch is only of the order of a few percent. In the calculations of the direct capture part, only E2 radiative transitions were assumed. This is, in principle, incomplete, as $2_i^+ \to 2_f^+$ transitions could also proceed via M1 radiation. However, in Ref. [58], the expected M1 matrix element is stated to be proportional to the magnetic moments of the particles in the transition, and thus should be zero for α and ^{12}C particles. Therefore a strong suppression of M1 (and other magnetic) isoscalar transitions is expected. Fig. 7 shows a possible energy dependence of the 6.9 MeV S-factor.

Fig. 7 shows the expected total S-factor (dashed) as well as its decomposition into incoming partial waves $\ell_i = 0$ (dotted), 1 (long dash-dot), 2 (short-dash-dot), 3 (double short dash), and 4 (triple short dash). It is obvious from Fig. 7 that the direct capture[15] or the

[15] As in Ref. [11] the hard-sphere (external part of the transition) cross section is ($\ell_f = 2$)

$$\sigma_{DC\to 6.9}(E) = \frac{\pi}{k^2} \sum_{\ell_i=0,2,4} (2\ell_i + 1)\left|U_{6.9}^{\ell_i}(E)\right|^2, \tag{13}$$

where k is the α-particle wave number and the scattering function is

$$U_{6.9}^{\ell_i}(E) = \frac{-6i}{\sqrt{10}} \frac{M_n^{1/2} e_q}{\hbar k} e^{i(\omega_{\ell_i} - \phi_{\ell_i})} P_{\ell_i}^{1/2} k_\gamma^{5/2} N_f^{1/2} a^2 F_{\ell_i}(a) G_{\ell_i}(a) i^{\ell_i} \theta_\alpha^{6.9}(\ell_i 200|20) J_2'(\ell_i, 2). \tag{14}$$

The summation extends over the three possible incoming angular momenta for E2 capture into the 6.9 MeV state, i.e., s-, d-, and g-wave (similar to Eq. (9)) Both N_f and $J_2'(\ell_i, 2)(E)$ which stem from the overlap between the wave function of the bound ground state and the external Coulomb functions are (similar to Eqs. (9) and (11)) as

$$N_f^{-1} = 1 + \frac{2(\theta_\alpha^{6.9})^2}{a} \int_a^\infty dr \left[\frac{W_2(r)}{W_2(a)}\right]^2 \tag{15}$$

and (see Eq. (11))

$$J_2'(\ell_i, 2)(E) = \frac{1}{a^3} \int_a^\infty r^2\, dr\, \frac{W_2(r)}{W_2(a)} \left[\frac{F_{\ell_i}(r)}{F_{\ell_i}(a)} - \frac{G_{\ell_i}(r)}{G_{\ell_i}(a)}\right]. \tag{16}$$

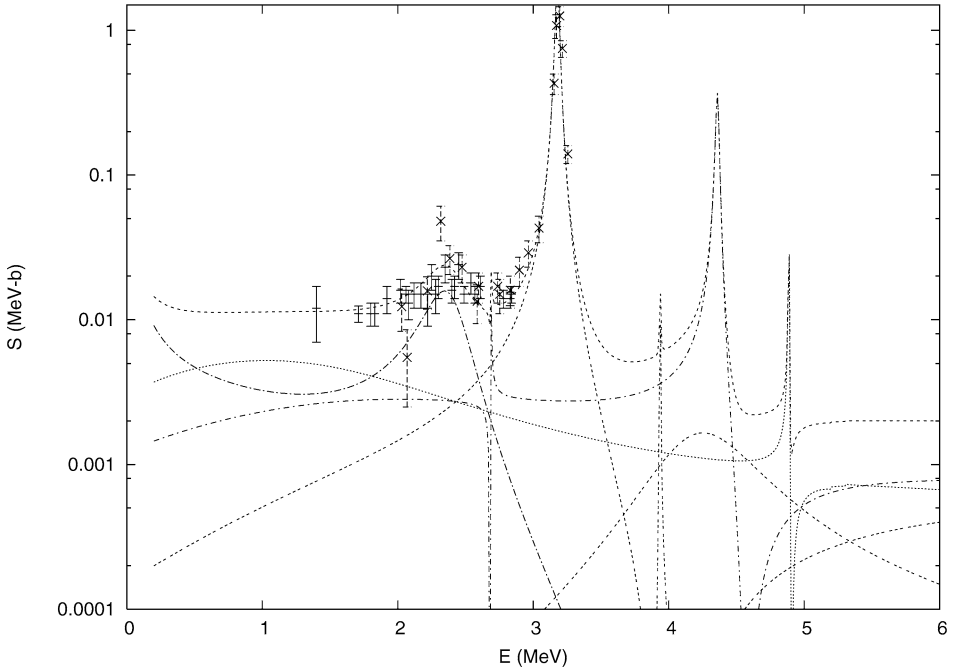

Fig. 7. R-matrix calculation of the S-factor section for the radiative capture into the 6.9 MeV state of ^{16}O and the data of Kettner et al. [45] (cross) and Redder et al. [46] (bar). The decomposition into incoherent parts of the cross section is shown as indicated, as well as the summed S-factor. The dashed curve shows the total S-factor. (For further discussion see text.)

$\ell = 1$ resonance capture dominates at low energies. The $\ell = 1$ resonance capture strength depends on the unknown transition strength of the $E = 7.1 \rightarrow 6.9$ MeV transition, which forms as in the ground state case a potential subthreshold resonance. More can be found in Ref. [59]. This S-factor is largely unknown. The more certain S-factor at low energies is the s-wave part of the direct capture. Because of the closeness to the α-threshold of the 6.9 MeV state, it shows a distinct maximum at astrophysical energies, typically being of the order from a few up to 10 keV b at $E = 300$ keV. The exact prediction may, however, depend on theory.

Kunz et al. [50] claimed that cascades were unimportant, as they saw little evidence for them, contrary to Refs. [45,46]. Also, their extrapolation led to very low values of $S_{\mathrm{casc}}(300)$. However, the extrapolation did not include any direct component [54]. The DRAGON measurements, however, have shown (Section 3.7.1) that there is a considerable

Note that $\theta^{6.9}$ is common to the three incoming partial waves in the summations of Eqs. (13). The reduced width amplitude in this case (Eq. (10)) $\gamma_{6.9}$ (aka γ_{12}) is related to the dimensionless reduced width via

$$\theta_{\alpha}^{6.9} = \gamma_{6.9}\left(\hbar^2/\mu a^2\right)^{-1/2} \tag{17}$$

with the reduced mass μ of the $^{12}\mathrm{C} + \alpha$ system.

cascade cross section down to below the 2.46 MeV 1^- resonance. It should be pointed out that the direct capture strength of the transition into the 6.9 MeV state is directly linked to the strength of the subthreshold resonance in the E2 ground state transition, see Section 3.7.3.

3.6.3. Capture to the 6.1 and 7.1 MeV states

There is no experimental evidence that there are cascade transitions through the 6.1 MeV state (3^-) in ^{16}O, except for the 4^+ resonance at 3.9 MeV, which is at relatively high energy and has a rather narrow width. The capture would be expected to proceed mainly via a p-wave and E2 transition at low energies. With the 7.1 MeV state having a strong transition (in W.U.) into the 6.1 MeV state, this state will act as a subthreshold resonance. At the $E = 2.46$ MeV 1^- resonance, only an upper limit is known for this transition. More data and theory will be required to estimated the strength of this transition.

The transition to the 7.1 MeV state has been estimated in Ref. [11] based on the data of [46] who found this transition in the 1^- resonance at $E = 2.46$ MeV. For reasons given in Section 3.2.1 and [25] we take the value of Ref. [11] using an interaction radius $a = 5.5$ fm. Thus $S_{7.1}(300) = 0.3$ keV b.

3.7. Future possibilities to improve the extrapolation of cross sections to low energies

3.7.1. Recoil separators

Typically measurements of the emitted γ rays in $^{12}\mathrm{C}(\alpha,\gamma)^{16}\mathrm{O}$ suffer from either neutrons (and their secondary capture γ emissions) produced at higher energies from α or ^{12}C beams, or from room background (cosmic rays or natural radioactivity) at lower beam energies. The additional detection of the recoiling ^{16}O particle does provide added orders of magnitude suppression of the these backgrounds.

There has been one published measurement of $^{12}\mathrm{C}(\alpha,\gamma)^{16}\mathrm{O}$ employing a recoil separator at Caltech [47]. As typical for recoil separators, major backgrounds in the focal plane were from beam particles leaking through the separator, transported through by multiple scattering of the beam. γ-recoil coincidences removed that problem; however, as mentioned earlier (Section 3.4) this separator had insufficient longitudinal acceptance. In general, the longitudinal and transverse acceptance has to increase with decreasing energies, and separators exceeding 35 mrad transverse and 7% energy acceptance may be ultimately desirable with beam to recoil suppressions of 10^{18} or better needed at the same time.

At present, at two such separators the measurement of the $^{12}\mathrm{C}(\alpha,\gamma)^{16}\mathrm{O}$ reaction is actively being pursued. These are ERNA (European Recoil separator for Nuclear Astrophysics) at the Ruhr Universität Bochum [60], and DRAGON (Detector for Recoils And Gammas of Nuclear reactions) at TRIUMF [61]. First results show that indeed very clean spectra can be obtained: see Fig. 8 as measured at the DRAGON facility. The DRAGON data also show that the angular distribution of the ground state decay, is reflected in the energetic recoil distribution which can be resolved with a detector of reasonable good resolution like a silicon detector.

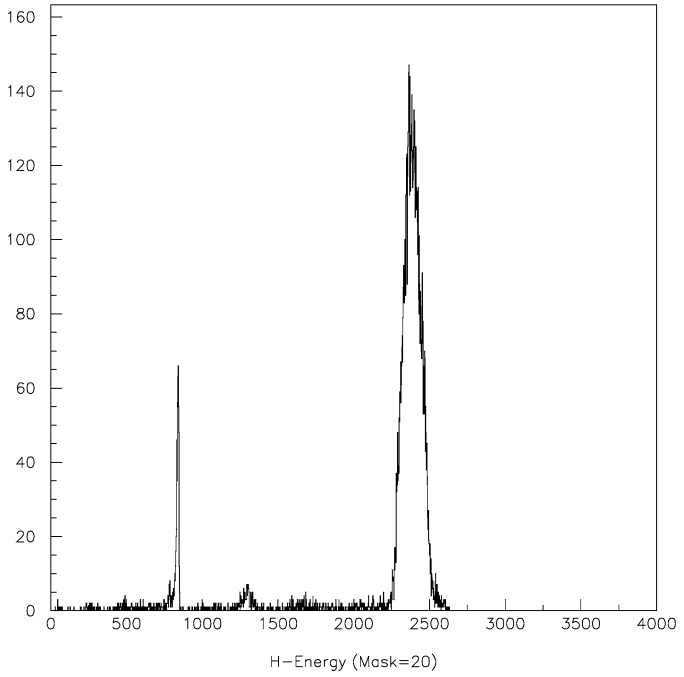

(a)

Fig. 8. Spectra from DRAGON [62]. (a) Single heavy ion spectrum at the $E = 5.278$ MeV resonance (channel number versus counts/channel). The peak around channel 750 results from an α source, while the peak at channel 2300 is the ^{16}O recoil peak. Events below this peak are due to the response of the segmented silicon detector used. (b) ^{16}O gated γ-spectrum from the BGO detectors surrounding the target for a low cross section. Ground state and cascade transitions are clearly visible.

3.7.2. Extension of the radiative capture cross section for the ground state to higher energies

At high beam energies, beam induced backgrounds become dominant in the γ spectra, terminating most γ-ray only measurements at energies slightly above 3 MeV. In this region, the S-factor of the 1^- ($E = 2.4$ MeV) resonance is decreasing steeply, and the E2 fraction becomes stronger and will, most likely, eventually be dominant. As it is dominant in strength, major restrictions on the direct part of the E2 capture and some interference signs in particular with the $E = 4.3$ MeV 2^+ resonance can be expected by knowledge of this energy region. The E1 part may become unmeasurable small in this region; however, it will increase steeply again as one approaches the 5.1 MeV 1^- resonance. This resonance interferes with the 2.4 MeV one, and most certainly the interference pattern can be deduced from cross section measurements, also allowing one to draw important conclusions on the low energy region. Also, as discussed in Section 3.5.3, the interference between the direct capture and the 2^+ resonance at 4.36 MeV can be measured directly. In summary, measurements at energies higher than presently achieved would be a direct complement to low energy measurements. Recoil separators are an ideal tool to achieve these measure-

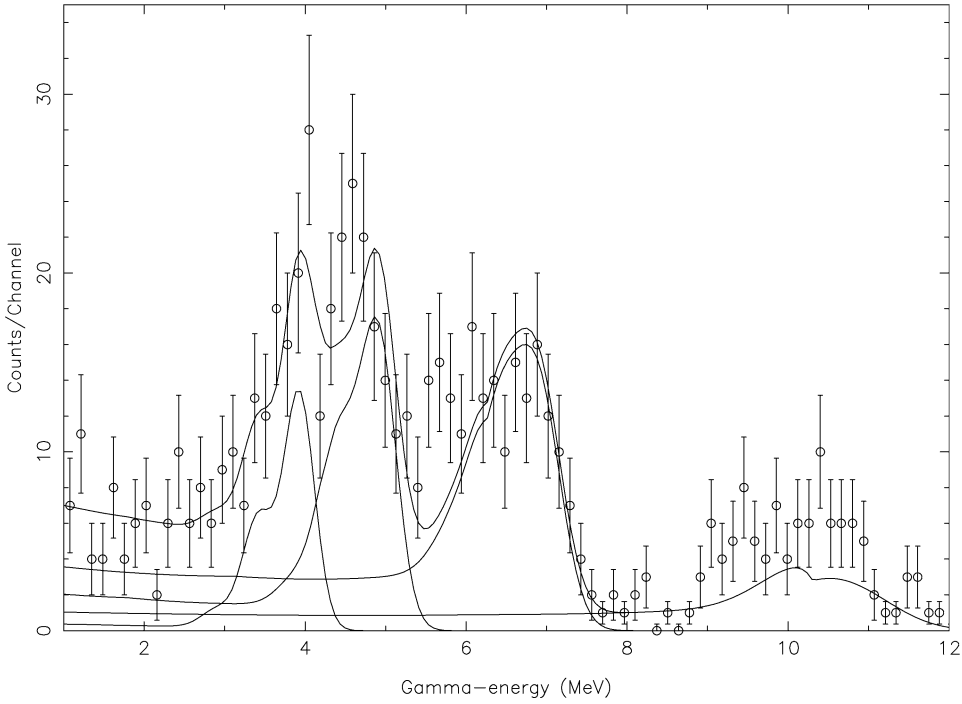

(b)

Fig. 8. (continued).

ments. Preliminary data from both ERNA [60] and DRAGON [61] are now available in this energy region.

3.7.3. Determination of the α-dimensionless reduced width, $\Theta_\alpha^{6.9}$, by cascade direct capture

For the cascade transition through the subthreshold 6.9 MeV $J^\pi = 2^+$ state (Section 3.6.2), the cross section is for many energies governed by the direct capture process for which the magnitude is directly given by the dimensionless α reduced width amplitude, $\theta_\alpha^{6.9}$, of the 6.9 MeV state which reflects the particle (α) properties of this state. Therefore a thorough measurement of the direct capture part of the cascade transition through the 6.9 MeV state could yield a precise determination of the α-width of this state.

The connection between the cascade transition through the 6.9 MeV state and the d-wave properties of ^{16}O was noted in Refs. [11,45,46], where separate and simultaneous fits for the d-wave elastic phase shift, the cascade S-factor and the radiative ground state E2 transition were employed in different contexts. Ref. [11] indeed connects resonance R-matrix parameters and the direct capture process in a self consistent way. It can indeed be shown [59] that the reduced α-width of the 6.9 MeV 2^+ state in ^{16}O can be uniquely determined (for a chosen channel radius a) by a measurement of the excitation function of the cascade transition through the 6.9 MeV state. It is therefore the magnitude of the cas-

cade cross section which directly gives the reduced α-width of the 6.9 state. Knowledge of this width will put the extrapolation of the E2 ground state transition on a more solid footing and will hopefully reach agreement with the elastic scattering data which seem to show somewhat lower values for the reduced α-width of the 6.9 MeV state in ^{16}O. This will reduce to a great extent this major uncertainty in the $^{12}\mathrm{C}(\alpha,\gamma)^{16}\mathrm{O}$ cross section at astrophysically important energies.

3.8. Derivation of the stellar reaction rate

Stellar reaction rates are derived by averaging the product of the velocity and the nuclear cross section over the Maxwell–Boltzmann distribution (Ref. [3])

$$\langle\sigma v\rangle = \left(\frac{8}{\pi\mu}\right)^{1/2}\left(\frac{1}{kT}\right)^{3/2}\int_0^\infty S(E)\exp\left[-\frac{E}{kT}-\frac{b}{E^{1/2}}\right]dE, \tag{18}$$

where μ is the reduced mass of the two particle system, k the Boltzmann constant, $b = 0.989 Z_1 Z_2 \mu^{1/2}$ and $Z_{1,2}$ the nuclear charges. With N_A Avogadro's number, $N_A\langle\sigma v\rangle$ is then either tabulated or given as an analytic expression in compilations of stellar reaction rates (e.g., [63]). For most cases the integral cannot be solved analytically.

In the compilations of stellar reaction rates initiated by Fowler [63–67] the analytic expression for the rate of $^{12}\mathrm{C}(\alpha,\gamma)^{16}\mathrm{O}$ consists of the sum of two to four terms (rational functions combined with exponentials) depending on the publication. The first term in [63] results from the tail of the $J^\pi = 1^-$, $E_x = 7.117$ MeV state, already present in Ref. [65]. In Ref. [66] it is reported that this term has been matched by numerical integration to the cross section extrapolation as performed in [43]. The second term of Ref. [63], only introduced in Ref. [67], is a term resulting from the $J^\pi = 2^+$, $E_x = 6.9$ MeV state. The third term is a narrow resonance expression for the $E_x = 9.6$ MeV state in ^{16}O, present since Ref. [65]. The fourth term was introduced Ref. [66] by summing higher resonances and has never been changed. The other terms have been altered in subsequent compilations according to newly available information. The fourth term is only important for temperatures[16] above $T_9 = 1.5$. Below this temperature the first two (subthreshold state) terms in [63] are the only ones of significance. In many cases (e.g., [68]) the rate of [63] has been scaled linearly with respect to $S(300)$ to incorporate different values of the $^{12}\mathrm{C}(\alpha,\gamma)^{16}\mathrm{O}$ cross sections. As long as one is only dealing with energies around 300 keV, equivalent to temperatures of $T_8 = 1$ in helium burning, this is a rather good approximation (though missing the subtleties introduced by cascade transitions). However, as higher temperatures are demanded in modeling, the tails of subthreshold resonances become less dominant in the reaction rate and the complexities of interfering nuclear processes have to be taken into account. Therefore, a more nearly correct way of obtaining these reaction rates is to numerically integrate Eq. (18) for all components of the $^{12}\mathrm{C}(\alpha,\gamma)^{16}\mathrm{O}$ cross section. This has been done in Ref. [69] for the cross sections available at the time. The reaction rates thus obtained have then been fitted to rational expressions as commonly used in stellar modeling programs. Meanwhile more cascade information has become available which needs to

[16] Stellar burning temperatures are given as $T_8 = T/10^8$ K and $T_9 = T/10^9$ K.

be more completely incorporated. However, since there are no other major changes to this rate, it still can be recommended. It should be remarked that this rate cannot, in principle, easily be scaled, as it is composed of several components with different energy and thus temperature dependences. Some scaling advice is given in Ref. [69].

3.9. Summary of the present status of $^{12}C(\alpha,\gamma)^{16}O$

In the last 30 years remarkable progress has been achieved in the determination of the $^{12}C(\alpha,\gamma)^{16}O$ cross section. Yet, major uncertainties remain in the extrapolation to low energies, particularly if precisions of 10% at 300 keV remain desirable [68]. In detail, the different components of the S-factor at 300 keV add up as follows: (i) $S_{E1}(300) = 80 \pm 20$ keV b with improvements possible by systematic work on the ^{16}N decay spectrum; (ii) $S_{E2}(300) = 53^{+13}_{-18}$ keV b from elastic scattering.[17] For the E2 ground state cross section the sign of the interference between direct capture and the tail of the 6.9 MeV state still needs better confirmation. We also note that the elastic scattering results and the direct capture result into the 6.9 MeV state do not agree. For cascade transitions, the one to the 6.9 MeV state appears to be the strongest. We recommend a best value of $S_{6.9}(300) = 7^{+13}_{-4}$ keV b; however, there is a chance, that $S_{6.9}(300)$ may be higher, if the 7.1 MeV state should conspire to contribute in a significant way. For the transition to the 6.0 MeV state with the detection of a signal (Section 3.6.1), one may estimate an S factor of $S_{6.0}(300) = 5^{+7}_{-4.5}$ keV b. As for the other cascade transitions they are likely so small that their contribution at 300 keV can be neglected. However, at higher energies/temperatures those and the other cascade contributions could easily become as strong as the ground state transitions. This feature certainly has to be further explored for stellar reaction rates of $^{12}C(\alpha,\gamma)^{16}O$ at temperatures beyond core helium burning.

4. He-burning reactions involved in neutron production

As noted earlier (Section 1), the production of nuclides with masses above those in the iron-nickel abundance peak is mainly the result of radiative capture of neutrons because the increasing Coulomb barrier severely inhibits production by charged particle induced reactions. As is now well known, there is clear evidence, from nuclear abundances, of neutron capture on a slow time scale[18] (relative to typical β-decay lifetimes) as well as for neutron captures on a rapid timescale[19]; these are known as the s-process and r-process, respectively [70]. Here we limit the discussion to the neutron producing reactions involved in the s-process.

[17] See, however, 81 ± 22 keV b for the Stuttgart extrapolation (Section 3.4).
[18] Discussed elsewhere in this volume.
[19] Discussed elsewhere in this volume.

4.1. The $^{13}C(\alpha, n)^{16}O$ reaction

Even within this limitation, there is good evidence for two principal neutron-production reactions, $^{13}C(\alpha, n)^{16}O$ and $^{22}Ne(\alpha, n)^{25}Mg$ that apparently share the build-up of most of the s-process nuclei. The build-up of nuclei with $A \lesssim 90$, the so-called weak component, is believed to occur during He-burning in massive stars with $M \geqslant 8$ solar, while the build-up of the main component (nuclei with $90 < A < 209$), is attributed to low-mass asymptotic giant branch (AGB) stars [71]. The lower temperatures in lower mass stars are more likely to produce neutrons by the $^{13}C(\alpha, n)$ reaction so that this reaction may produce about 95% of the total neutron exposure [71]. However, the $^{22}Ne(\alpha, n)$ reaction contributes neutrons in both low and large mass stars, and both of the neutron producing reactions appear to be necessary for a full understanding of the s-process.

The ^{13}C needed for the $^{13}C(\alpha, n)$ reaction is generally believed to be produced in thermally pulsing AGB stars which can mix a small amount of hydrogen from the hydrogen burning shell with ^{12}C from an inner helium-burning shell. Thus we can expect the reaction $^{12}C(p, \gamma)^{13}N$ followed by positron decay. The freshly made ^{13}C may now react with helium via the $^{13}C(\alpha, n)^{16}O$ reaction.

The cross section for the $^{13}C(\alpha, n)$ reaction, at temperatures near 10^8 K, may not be accurately known at this time, since there is a possibility of a subthreshold $J^\pi = 1/2^+$ resonance about 3 keV below the threshold. R-matrix analyses show a possible sharp upturn of the S-factor as the energy is lowered below the lowest cross section measured at $E = 0.28$ MeV [73]. However, the level of participation of the subthreshold resonance remains uncertain [72].

The $^{22}Ne(\alpha, n)^{25}Mg$ reaction depends on the availability of ^{22}Ne which is built by the He-burning reactions $^{14}N(\alpha, \gamma)^{18}F(\beta^+\nu)^{18}O(\alpha, \gamma)^{22}Ne$. The starting nucleus for this chain of reactions, ^{14}N, arises as the product of the C–N–O cycle of earlier hydrogen burning, in which the resulting products are mainly helium and ^{14}N, the nucleus with the smallest (p, γ) cross section. Some ^{14}N could also be produced in the AGB thermal pulsation by the reaction $^{13}C(p, \gamma)^{14}N$. In the latter case, it is important to recall that ^{14}N is a neutron "poison", i.e., the reaction $^{14}N(n, p)^{14}C$ has a relatively large cross section for capturing neutrons.

4.2. The $^{14}N(\alpha, \gamma)^{18}F$ reaction

The low energy resonances at $E = 446$ keV and 888.5 keV in the $^{14}N(\alpha, \gamma)^{18}F$ reaction were remeasured by Görres et al. [74] who present reaction rates based on these two resonances and the higher resonances cited by the compilation of Angulo et al. [73]. For $T < 7 \times 10^8$ K, the cross section is dominated by the resonance at $E = 446$ keV. However, at the lower temperatures there could be contributions from direct radiative capture to low-lying ^{18}F states, or from a resonance at $E = 237$ keV, in addition to the $E = 446$ keV resonance. These contributions had to be estimated. It seems, however, that at the temperatures reached in He-burning, the $^{14}N(\alpha, \gamma)$ reaction will convert the ^{14}N to ^{18}O within $\sim 10^5$ years, which is already faster than the following conversion of ^{18}O to ^{22}Ne.

4.3. The $^{18}O(\alpha,\gamma)^{22}Ne$ reaction

The most recent study of the $^{18}O(\alpha,\gamma)^{22}Ne$ reaction is that of Dabanek et al. [71]. This paper has reinvestigated the strengths of the lower energy resonances at $E = 384.5$, 463, 540 and 613.6 keV, and has chosen the strengths adopted by Angulo et al. [73] for higher resonances. The tabulated rates given by Dabanek et al. [71] differ a little from those tabulated by Angulo et al., but the changes are not major, as would be expected, since most of the resonance strengths have been carried over from Angulo et al.

4.4. The $^{22}Ne(\alpha,n)^{25}Mg$ reaction

The $^{22}Ne(\alpha,n)^{25}Mg$ reaction has been restudied from threshold at $E = 478$ keV to $E = 1227$ keV by Jaeger et al. in 2001 [75] with much larger beam currents than have been employed earlier. Most of the resonances seen in the newer work have been seen by other studies, but agreement between the studies is rather poor, especially at the low energies. In the compilation by Angulo et al. [73], the lowest resonance included is at $E = 704$ keV ($E_{lab} = 832$ keV) and a constant value for the S-factor was assumed from the base of the resonance down to the threshold. The newer work was able to establish considerably lower background levels than previously accomplished, and put an upper limit of $\omega\gamma < 60$ neV on a possible resonance at $E = 537$ keV, an order of magnitude smaller than the next larger upper limit, and two orders of magnitude below the backgrounds in other earlier studies.

The tabulated reaction rates from the Jaeger et al. work are about $\frac{1}{4}$ of the Angulo et al. rate at $T_8 = 1.2$, about $\frac{2}{3}$ of the Angulo et al. rate at $T_8 = 2.5$ and at $T_8 = 5$, and close to the same value at $T_9 = 1$. It should be noted that an improved measurement of the competing $^{22}Ne(\alpha,\gamma)^{26}Mg$ reaction is desirable.

5. Carbon, neon, oxygen and silicon burning

After core helium-burning, a star will be left with a core consisting mostly of carbon and oxygen, in a ratio determined by the relative cross sections for the triple-α process and the $^{12}C(\alpha,\gamma)^{16}O$ reaction that produces ^{16}O from some of the ^{12}C. The ratio of carbon to oxygen also depends on the core density as well as the temperature. As we noted earlier, the carbon to oxygen ratio at the end of helium burning strongly affects the succeeding nucleosynthesis of heavier elements in massive stars, and the eventual mass of the iron core resulting from silicon burning. As a result, the relationship between the kind of supernova remnant left and the initial stellar mass is also affected by the carbon–oxygen ratio at the end of helium burning [76].

5.1. Carbon burning

The first of the three "heavy-ion reactions", carbon burning, leads to a very short-lived intermediate nucleus ^{24}Mg, that breaks up mainly by emitting α particles, protons, or neutrons:

$$^{12}\mathrm{C} + {}^{12}\mathrm{C} \rightarrow {}^{24}\mathrm{Mg} \rightarrow {}^{20}\mathrm{Ne} + {}^{4}\mathrm{He} + 4.62\ \mathrm{MeV}$$
$$\rightarrow {}^{23}\mathrm{Na} + {}^{1}\mathrm{H} + 2.24\ \mathrm{MeV}$$
$$\rightarrow {}^{23}\mathrm{Mg} + \mathrm{n} - 2.60\ \mathrm{MeV}.$$

The neutron production is endoergic, and requires higher temperatures than the two other reactions. After the positron decay of ^{23}Mg, the existence of the neutron-producing channel has increased the neutron excess of the nuclides present, a quantity that continues to increase with later processes and affects the details of the nucleosynthesis.

The cross section for the $^{12}\mathrm{C} + {}^{12}\mathrm{C}$ reactions are known experimentally down to $E \approx 2.4$ MeV, about the upper edge of the Gamow peak at $T_9 \sim 0.8$, a typical temperature for carbon burning. It would be reassuring to have measured cross sections extending to somewhat lower energies (in particular for SN Ia ignition), but the cross section rapidly becomes more difficult to measure at low energies, and is increasingly sensitive to the beam energy and to the existence of prominent, overlapping resonances [77]. The measured cross sections have been fitted roughly by optical potential models [77]. In stellar evolution models it appears that the rates recommended by Caughlan and Fowler [63] are still used because there appear to be no newer experimental cross section data. The main products from carbon burning model calculations are, of course, ^{20}Ne and ^{24}Mg, the latter from $^{23}\mathrm{Na} + \mathrm{p}$; however, the range of nuclides produced includes also ^{21,22}Ne, ^{23}Na, ^{25,26}Mg, ^{26,27}Al, ^{28,29,30}Si and ^{31}P [76].

5.2. Neon burning

It might reasonably be presumed that oxygen burning would follow immediately after the consumption of carbon but, before the temperature becomes high enough to burn oxygen, the temperature is high enough to photodisintegrate neon with the high energy tail of the black body radiation. This occurs because ^{20}Ne has by far the lowest threshold among the abundant nuclei present for α particle photo-emission

$$^{20}\mathrm{Ne} + \gamma \rightarrow {}^{16}\mathrm{O} + \alpha - 4.73\ \mathrm{MeV}.$$

The freed α-particle can recombine with ^{16}O to reform ^{20}Ne, but can also capture on ^{20}Ne to form ^{24}Mg:

$$^{20}\mathrm{Ne} + \alpha \rightarrow {}^{24}\mathrm{Mg} + \gamma + 9.42\ \mathrm{MeV}.$$

These two reactions are energetically equivalent to

$$^{20}\mathrm{Ne} + {}^{20}\mathrm{Ne} \rightarrow {}^{16}\mathrm{O} + {}^{24}\mathrm{Mg} + 4.59\ \mathrm{MeV}.$$

The overall reaction products are similar to carbon burning (with the obvious exception of ^{20}Ne which is produced in carbon burning but destroyed in neon burning).

Since recently published measurements at Stuttgart [2] on the $^{16}\mathrm{O}(\alpha,\gamma)^{20}\mathrm{Ne}$ reaction have shown that the low energy cross section may be slightly higher than previously estimated, it is possible that the photodisintegration of ^{20}Ne may proceed at slightly lower temperature than previously surmised. However, such small changes would not affect the exclusion of $^{16}\mathrm{O}(\alpha,\gamma)^{20}\mathrm{Ne}$ from core He-burning.

5.3. Oxygen burning

After most of the core neon has been destroyed, the core temperature will rise to $T_9 \sim 2$ where oxygen can burn in the reactions

$$\begin{aligned} {}^{16}\mathrm{O} + {}^{16}\mathrm{O} \rightarrow {}^{32}\mathrm{S} &\rightarrow {}^{28}\mathrm{Si} + {}^{4}\mathrm{He} + 9.59\ \mathrm{MeV} \\ &\rightarrow {}^{31}\mathrm{P} + {}^{1}\mathrm{H} + 7.68\ \mathrm{MeV} \\ &\rightarrow {}^{31}\mathrm{S} + \mathrm{n} + 1.50\ \mathrm{MeV} \\ &\rightarrow {}^{30}\mathrm{Si} + 2\mathrm{p} + 0.38\ \mathrm{MeV} \\ &\rightarrow {}^{30}\mathrm{P} + {}^{2}\mathrm{H} - 2.41\ \mathrm{MeV}. \end{aligned}$$

The released α particles, protons and neutrons can produce a wide range of nuclei, including in addition to those listed, ${}^{33,34}\mathrm{S}$, ${}^{35,37}\mathrm{Cl}$, ${}^{36,38}\mathrm{Ar}$, ${}^{39,41}\mathrm{K}$, ${}^{40,42}\mathrm{Ca}$, ${}^{44}\mathrm{Ti}$ and ${}^{50}\mathrm{Cr}$, with ${}^{28}\mathrm{Si}$ and ${}^{32}\mathrm{S}$ the main products [76]. The large spread of nuclei is partly due to the increase of the neutron excess during core oxygen burning from $\sim 2 \times 10^{-3}$ to $\sim 10^{-2}$ [78]. At a neutron excess this large, the predicted distribution of product nuclei and isotopes would disagree with observed matter [78]. It would therefore appear that the products of core oxygen burning are rarely dispersed into space. Oxygen shell burning can proceed at higher temperatures (and lower densities), producing a distribution of isotopes in better agreement with observed matter [76].

There have been no recent experiments to measure the cross section for oxygen burning. However, the statistical model fit of Caughlan and Fowler [63] and Hartree–Fock model calculations by Reinhard et al. [79] agree within a factor of two and cover the temperature region ($T_9 \approx 3$–3.9) needed for explosive oxygen burning, and much of the region ($T_9 \sim 2$) needed for core oxygen burning. The Caughlan–Fowler rates remain in use for current stellar models. It is clear that renewed efforts to extend the range of the cross section measurements, and to verify existing measurements are needed. With improved experimental results, it should be possible to substantially improve the optical model theoretical fits as well.

5.4. Silicon burning

By the time silicon burning begins, a quasiequilibrium cluster of isotopes, built up by the joining of smaller clusters, has reached from $A \sim 26$ to $A \sim 46$, and there is a growing cluster of isotopes in the region of the iron abundance peak. Because of the rising temperature, the nuclei continue to built up to the region of maximum nuclear binding energy by proton, neutron, and α particle induced nuclear reactions. The source of these particles is the photodisintegration of the more abundant lighter nuclei such as ${}^{28}\mathrm{Si}$.[20] This build-up continues until most of the core nuclei eventually reach the iron group, via a quasiequilibrium cluster extending from the protons and neutrons to the iron group isotopes of iron and nickel [81].

[20] There is a new measurement of the ${}^{24}\mathrm{Mg}(\alpha,\gamma){}^{28}\mathrm{Si}$ reaction in progress which has so far discovered two new low energy resonances [80].

Because of the growing neutron excess (up to 0.07), the most abundant nuclide would be ^{56}Fe. However the most abundant nuclide with an equal neutron-proton number would be ^{56}Ni. Interestingly, γ-rays from SN 1987a, detected by high altitude balloon flights and satellite γ-ray-detectors, include those from ^{56}Ni, ^{56}Co, and ^{57}Co positron decays [82]. The ^{56}Ni is a signal that the elemental build-up occurred quickly, with little time for the development of a significant neutron excess, as one might expect from a supernova explosion. Much of the matter carried all the way through core hydrostatic burning must be trapped in supernova remnants, as observed nuclidic ratios in matter are not well fitted by the predicted final results of the most advanced core hydrostatic burning. A more plausible source for the nuclidic composition from advanced burning process may be explosive shell burning during supernova explosions.

From the laboratory point of view a large number of charged particle reaction studies have been carried out over many years, and measurements continue mainly for nuclei lighter than iron. Also, measured neutron radiative capture cross sections exist over the whole range of stable nuclei, and have enabled nuclear astrophysicists to discuss the s- and r-processes of neutron capture in considerable detail, even with complex branchings in successive neutron captures.

The measured nuclear reaction cross sections have served as guides for, and tests of efforts to develop theoretical expressions for nuclear reaction cross sections, as a function of the energy of the reacting nuclei, covering most of the chart of the nuclides [83]. Such theoretical attempts are not able to cope with nuclear reactions that have contributions from only a few scattered resonances as a function of energy, as occur in the lighter nuclei or close to the limits of nuclear stability. However, for nuclei with appreciable densities of energy levels at the interaction energies where cross sections are desired, theoretical cross section models have allowed enormous progress to be made in studying nucleosynthesis and stellar nuclear evolution. Contributing to those successes are the remarkable developments in computer speed that allow simultaneous handling of thousand of nuclides with ~ 1000 structural zones and 2000 timesteps for each nuclide [83].

6. Concluding remarks

To match these remarkable theoretical and computational advances, we need more and better experimental measurements, both for the cases where nuclear level densities are too low for nuclear reaction rates to be predicted with confidence, and also to allow improvements to be made in the theoretical predicted nuclear reaction rates. For example, we need to improve the parameters that are needed for nuclear reaction models for nuclei far from the locus of the stable nuclei.

We must also expect that stellar modelers will eventually ask for higher temperature cross sections for nuclear reactions among the lighter nuclei as they press forward in their growing understanding of stellar evolution. Many of these reactions, e.g., the triple-α reaction, will present serious challenges to the ingenuity of the experimentalists because obtaining the needed nuclear information could prove to be difficult.

Note added in proof

During the publication process of the present article, a paper has been published by Fynbo et al. [Nature 433 (2005) 136] extending their earlier work on the β-delayed α particles from ^{12}B and ^{12}N [9]. The new work finds evidence for a 0^+ ^{12}C state at (11.23 ± 0.05) MeV with a width of (2.5 ± 0.2) MeV, and a 2^+ state at (13.9 ± 0.3) MeV with a width of (0.7 ± 0.3) MeV. The article concludes that, for the temperature range $T_8 = 1$–10, the triple-alpha reaction rate remains well determined by the ^{12}C 7.65 MeV (resonance) state. For higher and lower temperatures, Fynbo et al. recommend changes from the rates given by the NACRE compilation [73]. As we have noted in the present paper, the γ-ray widths for higher energy resonances, and thus for the reaction rates, remain very uncertain. The value of the γ-width for the two higher resonances used in Fynbo et al. is likely close to the maximum possible value (K.P. Jackson, private communication) and therefore the stellar rate resulting from these resonances alone may be close to an upper limit. In addition, partial waves higher than s-waves, and also the changed population of the ^{8}Be with temperature have to be taken into account. For lower temperatures more sophisticated calculations of the ^{8}Be population than in Ref. [10], have to be carried out and direct E2 capture from an s-wave into the low-lying 2^+ ^{12}C state may be significant. Because of these large uncertainties in the rates at higher and lower temperatures, we have not revised the discussion in Sections 2.2 and 2.3 of the present paper.

Acknowledgements

The authors would like to thank S.E. Woosley for helpful discussions over many years. One of the authors, (C.A.B.), would like to thank J.W. Hammer and A. Lefebvre-Schuhl for sending preprints of references [52] and [53], respectively. The research of L.R. Buchmann is supported by TRIUMF and the Natural Sciences and Engineering Research Council of Canada, and the research of C.A. Barnes is supported in part by the California Institute of Technology.

References

[1] C.J. Hansen, S.D. Kavaler, Stellar Interiors, Springer, New York, 1994.
[2] A. Mayer, Doctoral thesis, Stuttgart, 2001;
J.W. Hammer, I. Büsching, M. Jaeger, R. Kunz, M. Mayer, R. Morlock, R. Schreiter, G. Staudt, P. Mohr, Y. Butt, P.D. Parker, K.-L. Kratz, B.P. Pfeifer, AIP Conf. Proc. 529 (2000) 669.
[3] C.E. Rolfs, W.S. Rodney, Cauldrons in the Cosmos, Univ. of Chicago Press, Chicago, 1988.
[4] H. Crannel, T.A. Griffy, L.R. Suelzle, M.R. Yearian, Nucl. Phys. A 90 (1967) 152.
[5] S. Woosley, private communication, 2003.
[6] H. Crannel, X. Jiang, J.T. O'Brien, D.I. Sober, E. Offermann, Nucl. Phys. A 758 (2005) 399c.
[7] S. Austin, Nucl. Phys. A 758 (2005) 375c.
[8] F. Ajzenberg-Selove, Nucl. Phys. A 506 (1990) 1.
[9] H.O.U. Fynbo, U.C. Bergman, M.J. Borge, P. Dendooven, C.Aa. Diget, W. Huang, J. Huikari, H. Jeppesen, B. Jonson, P. Jones, M. Meister, G. Nyman, Y. Prezado, K. Riisager, I. Storgaard Vogelius, O. Tengblad, Y. Wang, L. Weissman, K. Wilhelmsen Rolander, J. Äystö, Nucl. Phys. A 718 (2003) 541c.

[10] K. Nomoto, F.-K. Thielemann, S. Miyaji, Astron. Astrophys. 149 (1985) 239.
[11] F.C. Barker, T. Kajino, Aust. J. Phys. 44 (1991) 369.
[12] R.W. Hill, Phys. Rev. 90 (1953) 845.
[13] J.W. Bittner, R.D. Moffat, Phys. Rev. 96 (1954) 374.
[14] C.M. Jones, G.C. Phillips, R.W. Harris, E.H. Beckner, Nucl. Phys. 37 (1962) 1.
[15] J.D. Larson, T.A. Tombrello, Phys. Rev. 147 (1966) 760.
[16] G.J. Clark, D.J. Sullivan, P.B. Treacy, Nucl. Phys. A 110 (1968) 481.
[17] J.M. Morris, G.W. Kerr, T.R. Ophel, Nucl. Phys. A 112 (1968) 97.
[18] T.P. Marvin, P.P. Singh, Nucl. Phys. A 180 (1972) 282.
[19] F. Brochard, P. Chevallier, D. Disdier, V. Rauch, F. Scheibling, J. Phys. 36 (1975) 113.
[20] M. D'Agostino Bruno, I. Massa, A. Uguzzoni, G. Vannini, Nuovo Cimento A 27 (1975) 1.
[21] A.D. Frawley, J.D. Fox, K.W. Kemper, L.C. Dennis, Phys. Rev. C 25 (1982) 2935.
[22] M.A. Kovash, R.W. Lourie, W. Pugh, C.E. Hyde-Wright, D.G. Marchlenski, H.R. Suiter, J.C. Brown, R.G. Seyler, Phys. Rev. C 31 (1985) 1065.
[23] R. Plaga, H.W. Becker, A. Redder, C. Rolfs, H.P. Trautvetter, Nucl. Phys. A 465 (1987) 291.
[24] S.Y. Tong, W.N. Lennard, P.F.A. Alkemade, I.V. Mitchell, Nucl. Instrum. Methods B 45 (1990) 30.
[25] P. Tischhauser, R.E. Azuma, L. Buchmann, R. Detwiller, U. Giesen, J. Görres, M. Heil, J. Hinnefeld, F. Käppler, J.J. Kolata, H. Schatz, A. Shotter, E. Stech, S. Vouzoukas, M. Wiescher, Phys. Rev. Lett. 88 (2002) 072501.
[26] R. Plaga, Diplomarbeit, Universität Münster, 1986.
[27] L. Buchmann, R.E. Azuma, C.A. Barnes, J. Humblet, K. Langanke, Phys. Rev. C 54 (1996) 354.
[28] R.E. Azuma, L. Buchmann, F.C. Barker, C.A. Barnes, J.M. D'Auria, M. Dombsky, U. Giesen, K.P. Jackson, J.D. King, R.G. Korteling, P. McNeely, J. Powell, G. Roy, J. Vincent, T.R. Wang, S.S.M. Wong, P.R. Wrean, Phys. Rev. C 50 (1994) 1194;
An initial report was given in: L. Buchmann, R.E.. Azuma, C.A. Barnes, J. D'Auria, M. Dombsky, U. Giesen, K.P. Jackson, J.D. King, R. Korteling, P. McNeely, J. Powell, G. Roy, J. Vincent, T.R. Wang, S.S.M. Wong, P.W. Wrean, Phys. Rev. Lett. 70 (1993) 726.
[29] H. Hättig, K. Hünchen, P. Roth, H. Wäffler, Nucl. Phys. A 137 (1969) 144.
[30] H. Hättig, K. Hünchen, H. Wäffler, Phys. Rev. Lett. 25 (1970) 941.
[31] K. Neubeck, H. Schober, H. Wäffler, Phys. Rev. C 10 (1974) 320.
[32] H. Wäffler, private communications to C.A. Barnes, F.C. Barker, 1971.
[33] C.A. Barnes, Post deadline paper, in: Nucl. Phys. Div. Meeting, Santa Fe, NM, 1998;
R.E. Azuma, L. Buchmann, F.C. Barker, C.A. Barnes, J.M. D'Auria, M. Dombsky, U. Giesen, K.P. Jackson, J.D. King, R.G. Korteling, P. McNeely, J. Powell, G. Roy, J. Vincent, T.R. Wang, S.S.M. Wong, P.R. Wrean, Phys. Rev. C 56 (1997) 1655.
[34] H. Wäffler, private communication to C.A. Barnes, 16 December 1997.
[35] X. Ji, B.W. Filippone, J. Humblet, S.E. Koonin, Phys. Rev. C 41 (1990) 1736, and references therein.
[36] Z. Zhao, R.H. France III, K.S. Lai, S.L. Rugari, M. Gai, E.L. Wilds, Phys. Rev. Lett. 70 (1993) 2066.
[37] Z. Zhao, thesis, Yale University, 1993.
[38] Z. Zhao, Invited paper presented at the American Chemical Society Meeting in San Diego, March 1994.
[39] F.C. Barker, Aust. J. Phys. 24 (1971) 777.
[40] R.H. France III, E.L. Wilds, N.B. Jevtic, J.E. McDonald, M. Gai, Nucl. Phys. A 621 (1997) 165c.
[41] R.H. France III, thesis, Yale University, 1997.
[42] G.M. Hale, Nucl. Phys. A 621 (1997) 177c.
[43] P. Dyer, C.A. Barnes, Nucl. Phys. A 233 (1974) 495.
[44] T.R. Ophel, A.D. Frawley, P.B. Treacy, K.H. Bray, Nucl. Phys. A 273 (1976) 397.
[45] K.U. Kettner, H.W. Becker, L. Buchmann, J. Gőrres, H. Krăwinkel, C. Rolfs, P. Schmalbrock, H.P. Trautvetter, A. Vlieks, Z. Phys. A 308 (1982) 73.
[46] A. Redder, H.W. Becker, C. Rolfs, H.P. Trautvetter, T.R. Donoghue, T.C. Rinkel, J.W. Hammer, K. Langanke, Nucl. Phys. A 462 (1987) 385.
[47] R.M. Kremer, C.A. Barnes, K.H. Chang, H.C. Evans, B.W. Filippone, K.H. Hahn, L.W. Mitchell, Phys. Rev. Lett. 60 (1988) 1475.
[48] J.M.L. Ouellet, N. Butler, H.C. Evans, H.W. Lee, J.R. Leslie, J.D. MacArthur, W. McLatchie, H.-B. Mak, P. Skensved, J.L. Whitton, X. Zhao, Phys. Rev. C 4 (1996) 1982.

[49] G. Roters, C. Rolfs, F. Strieder, H.P. Trautvetter, Eur. Phys. J. A 6 (1999) 451.
[50] R. Kunz, M. Jaeger, A. Mayer, J.W. Hammer, G. Staudt, S. Harissopulos, T. Paradellis, Phys. Rev. Lett. 86 (2001) 3244.
[51] R. Kunz, M. Fey, M. Jaeger, A. Mayer, J.W. Hammer, G. Staudt, S. Harissopulos, T. Paradellis, Astrophys. J. 567 (2002) 643.
[52] J.W. Hammer, M. Fey, R. Kunz, J. Kiener, V. Tatischeff, F. Haas, J.L. Weil, M. Assunção, C. Beck, C. Boukari-Pelissie, A. Coc, J.J. Correia, S. Courtin, F. Fleurot, E. Galanopoulos, C. Grama, F. Hammache, S. Harissopulos, A. Korichi, E. Krmpotiĉ, D. Le Du, A. Lopez-Martens, D. Malcherek, R. Meunier, P. Papka, T. Paradellis, M. Rousseau, N. Rowley, G. Staudt, S. Szilner, Nucl. Phys. A 758 (2005) 363c.
[53] M. Assunção, M. Fey, A. Lefebvre-Schuhl, J. Kiener, V. Tatischeff, J.W. Hammer, C. Beck, C. Boukari-Pelissie, A. Coc, J.J. Correia, S. Courtin, F. Fleurot, E. Glanopoulos, C. Grama, F. Hass, F. Hammache, F. Hannachi, S. Harissopoulos, A. Korichi, R. Kunz, D. LeDuc, A. Lopez-Marteros, D. Malcherek, R. Meunier, Th. Paradellis, M. Rousseau, N. Rowley, G. Staudt, S. Szilner, J.P. Thibaud, J. Weil, Phys. Rev. C (2004), in press.
[54] W. Hammer, private communication, 2004.
[55] K. Langanke, C. Rolfs, Z. Phys. A 325 (1986) 193;
C.A. Barnes, K.H. Chang, T.R. Donoghue, C. Rolfs, J. Kammerad, Phys. Lett. B 197 (1987) 315.
[56] D.R. Tilley, H.R. Weller, C.M. Cheves, Nucl. Phys. A 564 (1993) 1.
[57] J.-M. Sparenberg, in: Proceedings of the 8th Symposium, Nuclei in the Cosmos, Nucl. Phys., in press;
J.-M. Sparenberg, Phys. Rev. C. 69 (2004) 034601.
[58] R.J. Holt, H.E. Jackson, R.M. Laszewski, J.E. Monohan, J.R. Specht, Phys. Rev. C 18 (1978) 1962.
[59] L. Buchmann, Phys. Rev. C 64 (2001) 022801.
[60] D. Schürmann, A. Di Leva, N. De Cesare, L. Gialanella, C. Imbriani, C. Lubritto, A. Ordine, V. Roca, H. Röcken, C. Rolfs, D. Rogalla, M. Romano, F. Schümann, F. Strieder, F. Terassi, H.P. Trautvetter, Nucl. Phys. A 758 (2005) 367c.
[61] D.A. Hutcheon, S. Bishop, L. Buchmann, M.L. Chatterjee, A.A. Chen, J.M. D'Auria, S. Engel, D. Gigliotti, U. Greife, D. Hunter, A. Hussein, C.C. Jewett, N. Khan, M. Lamey, A.M. Laird, W. Liu, A. Olin, D. Ottewell, J.G. Rogers, G. Roy, H. Sprenger, C. Wrede, Nucl. Instrum. Methods A 498 (2003) 190.
[62] L. Buchmann et al., E952 Collaboration, Experiment approved at TRIUMF, 2002.
[63] G.R. Caughlan, W.A. Fowler, At. Data Nucl. Data Tables 40 (1988) 283, here abbreviated CF88.
[64] G.R. Caughlan, W.A. Fowler, M.J. Harris, B.A. Zimmerman, At. Data Nucl. Data Tables 32 (1985) 197.
[65] W.A. Fowler, G.R. Caughlan, B.A. Zimmerman, Annu. Rev. Astron. Astrophys. 5 (1967) 525.
[66] W.A. Fowler, W.A. Caughlan, B.A. Zimmerman, Annu. Rev. Astron. Astrophys. 13 (1975) 69.
[67] M.J. Harris, W.A. Fowler, G.R. Caughlan, B.A. Zimmerman, Annu. Rev. Astron. Astrophys. 21 (1983) 1965.
[68] T.A. Weaver, S.E. Woosley, Phys. Rep. 227 (1993) 65.
[69] L. Buchmann, Astrophys. J. 468 (1996) L127;
L. Buchmann, Astrophys. J. 479 (1997) L153.
[70] E.M. Burbidge, G.R. Burbidge, W.A. Fowler, F. Hoyle, Rev. Mod. Phys. 29 (1957) 547.
[71] S. Dababneh, M. Heil, F. Käppler, J. Görres, M. Wiescher, R. Reifarth, H. Leiste, Phys. Rev. C 68 (2003) 025801.
[72] S. Kato, K. Abe, S. Kubono, T. Teranishi, M. Kurokawa, X. Liu, P. Strasser, N. Imai, K. Kumagai, C.S. Lee, Y.K. Kwon, C. Lee, J.H. Ha, Y.K. Kim, M.H. Tanaka, Y. Fuchi, Nucl. Phys. A 718 (2003) 189c.
[73] NACRE Collaboration, C. Angulo, et al., Nucl. Phys. A 656 (1999) 3.
[74] J. Görres, C. Arlandi, U. Giesen, M. Heil, F. Käppler, H. Leiste, E. Stech, M. Wiescher, Phys. Rev. C 62 (2000) 055801.
[75] M. Jaeger, R. Kunz, A. Mayer, J.W. Hammer, G. Staudt, K.L. Kratz, B. Pfeifer, Phys. Rev. Lett. 87 (2001) 202501.
[76] S.E. Woosley, A. Heger, Rev. Mod. Phys. 74 (2002) 1015.
[77] See, e.g., C.A. Barnes, S. Trentalange, S.C. Wu, in: D.A. Bromley (Ed.), Treatise on Heavy-Ion Science, vol. 6, Plenum, New York, 1985.
[78] S.E. Woosley, W.D. Arnett, D.D. Clayton, Astrophys. J. 175 (1972) 731.
[79] P.-G. Reinhard, J. Friedrich, K. Goeke, P. Grümmer, D.H.E. Gross, Phys. Rev. C 30 (1984) 878.
[80] M. Wiescher, private communication, 2004.
[81] See, for example, [78].

[82] See, for example, Matz, et al., Nature 331 (1988) 416;
Rester, et al., Astrophys. J. 342 (1988) L71;
Mahoney, et al., Astrophys. J. 334 (1989) L81;
Sandie, et al., Astrophys. J. 342 (1998) L91;
Teegarden, et al., Nature 339 (1989) 122.
[83] See, for example, T. Rauscher, A. Heger, R.D. Hoffman, S.E. Woosley, Astrophys. J. 576 (2002) 323, and references therein.